WULLENWEBBER ANTENNA VIBRATION STUDY.

RICHARD L. BRECKON
and
PHILIP R. HITE

WULLENWEBBER ANTENNA

VIBRATION STUDY

* * * * *

Richard L. Breckon

and

Philip R. Hite

WULLENWEBBER ANTENNA

VIBRATION STUDY

by

Richard L. Breckon

Lieutenant, United States Navy

and

Philip R. Hite

Lieutenant, United States Navy

Submitted in partial fulfillment of
the requirements for the degree of

MASTER OF SCIENCE
IN
AERONAUTICAL ENGINEERING

United States Naval Postgraduate School
Monterey, California

1 9 6 5

WULLENWEBBER ANTENNA

VIBRATION STUDY

by

Richard L. Breckon

and

Philip R. Hite

This work is accepted as fulfilling

the thesis requirements for the degree of

MASTER OF SCIENCE

IN

AERONAUTICAL ENGINEERING

from the

United States Naval Postgraduate School

ABSTRACT

The U. S. Navy is completing a world-wide radio directional antenna system, which has exhibited an undesirable wind induced oscillation of one of the primary structural members, resulting in physical damage and failure. This member is a horizontal beam 28 to 58 feet in length, supported 100 feet above ground, from which eight to 16 vertical wires are suspended. Oscillations at some installations have been estimated at six cycles per second, and with amplitudes of plus or minus two feet.

A dynamic wind tunnel model was designed, fabricated and tested, with the purpose of simulating the response of the various antenna designs. The installation at Winter Harbor, Maine, a two foot cylinder with one inch flanges at 90 degrees from the stagnation points, was investigated. These tests prove that, as a result of the flanges, the oscillation frequency is a function of wind velocity, so that the Strouhal number remains constant at 0.17. It is also shown that the structure's natural frequency has negligible effect upon response.

As an "in the field" modification, it is recommended that the beams be rotated 90 degrees about their longitudinal axes, which should reduce the amplitude of vibration by a factor of about six.

This study was conducted by Lieutenant Richard L. Breckon, USN, and Lieutenant Philip R. Hite, USN, at the United States Naval Postgraduate School, Monterey, California.

TABLE OF CONTENTS

Section	Title	Page
1.	Introduction	1
2.	Description of Model and Equipment	5
3.	Model Scaling	8
4.	Test Procedures	9
5.	Results	11
6.	Conclusions	17
7.	Bibliography	18
Appendix		
A.	General Antenna Information	35
B.	Wind Tunnel Test Section Calibration	39
C.	Accelerometer Calibration	43
D.	Response of a Cylinder to a Random Aerodynamic Forcing Function	47
E.	Test Data and Results	58
F.	Model Specifications	66

LIST OF ILLUSTRATIONS

Figure		Page
1.	Antenna Installation - General Layout	19
2.	Boom Boards	
	A. Circular (Winter Harbor, Maine)	20
	B. Rectangular (General)	20
3.	Model Detail	
	A. Schematic of Model Assembly	21
	B. Flexure Plate	21
	C. Adjustable Block	22
	D. Spring Bar Joint	22
4.	Complete Installation	23
5.	Block Diagram of Instrumentation	24
6.	Model Configuration	
	A. Configuration B	25
	B. Configuration C	25
	C. Configuration D	25
7.	Base Pressure Pickup	26
8.	Brush Recorder Tracing of Static Test	26
9.	Spring Bar Calibration	27
10.	Base Pressure Coefficient	28
11.	Oscillograph Trace of Configuration B	29
12.	Oscillograph Trace of Configuration C	29
13.	Oscillograph Trace of Configuration D	29

14. Dynamic Response

A. Configurations B,C,D at f_N = 20 cps 30

B. Configurations B,C at f_N = 30 cps 31

C. Configurations B,C at f_N = 40 cps 32

D. Configurations B,C at f_N = 50 cps 33

15. Model Response Frequency vs. Velocity (Configuration C) 34

A-1. Air Photograph of Honolulu Antenna 38

B-1. Wind Tunnel Pressure Survey 41

B-2. Wind Tunnel Operating Conditions 42

C-1. Endevco Accelerometer Calibration 46

D-1. Normalized Power Spectral Density 54

D-2. Smooth Cylinder Response Comparison 56-57

TABLE OF SYMBOLS

a	- acceleration
A	- projected area of cylinder = length x diameter
C_L	- lift/qA = lift coefficient
C_{P_B}	- $(P_b - P_o)/q$ = coefficient of base pressure
d	- cylinder diameter
f	- frequency, cycles per second (cps)
$L(t)$	- unsteady lift force, pounds
ℓ_B	- spring bar length, inches
m	- mass, slugs
P_b	- base pressure, pounds per square foot (psf)
P_o	- test section static pressure, psf
q	- $\rho V^2/2$ = dynamic pressure of fluid flow, psf
R	- Vd/ν= Reynolds number
RMS	- root-mean-square
S	- fd/V = Strouhal number
V	- velocity of undisturbed flow, feet per second (fps)
$y(t)$	- dynamic response deflection
$Z(i\omega)$	- complex impedance
β	- ratio of damping to critical damping
ρ	- density of fluid
ν	- kinematic viscosity
θ	- angular position around circumference of cylinder measured from front stagnation point, degrees
$\phi(\omega)$	- power spectral density of $\overline{L^2(t)}$
ω	- frequency, radians per second

ω_N - natural frequency, radians per second

Note: The mean square response is indicated as follows:

$$\overline{Z^2} = \lim_{T \to \infty} \frac{1}{2T} \int_{-T}^{+T} [Z(t)]^2 dt$$

1. Introduction.

The United States Navy is in the process of constructing a world-wide directional antenna system composed of 14 installations, of which nine have been completed to date. These antennas geometrically approximate a large cylindrical shape with a vertical axis of symmetry, and with the outer vertical surface acting as a radio wave reflector. The periphery of the cylinder is approximated by a number of straight segments, each of which is composed of two support towers and a horizontal member. This horizontal member, termed the boom board, supports a number of vertical reflecting wires which are connected at ground level through spring attachments.

The general antenna layout is presented in Figure 1. Dimensions vary considerably among installations, however the basic physical arrangement is uniform. Design of the individual components, such as support towers, boom boards, and attachment fittings, is at the option of the local contractor and consequently varies considerably from location to location. Appendix A lists the 14 locations, with remarks concerning individual designs.

Under certain wind conditions, the boom boards which are oriented with their longitudinal axis approximately perpendicular to the wind direction develop large amplitude (plus or minus two feet) vibrations. These vibrations have caused substantial damage to the vertical wires and their supporting attachments, and in extreme cases have resulted in physical failure of the boom board. For proper operation of the antenna, the vertical wires must remain within one degree of the vertical, so that any vibration which allows the wires to bow is undesirable. Ideally the boom board structure may be visualized as a constant

cross-section beam supported with some unknown degree of end-fixity (probably close to a simple support), with an evenly spaced elastic (spring) load over its length, acted upon by an unknown aerodynamic forcing function which is probably random in nature as a result of the steady wind and gusts.

The boom boards have in common the feature of being bluff bodies. By this is meant that the flow does not progress smoothly over the body, but rather separates from the surface in an unsteady manner, which in turn gives rise to the generation of fluctuating air loads that are as yet not predictable by theory. This is in contrast to the classic flutter situation for an airfoil where the loads may be derived by potential flow theory, and it is the phase difference between the motion and the air load which introduces energy into the system. The air loads on bluff bodies are random natured with the RMS amplitude of the response increasing with increased wind velocity. This random forcing function, coupled with light aerodynamic damping in the structure, causes a band-pass filter type reaction by the body. The structure usually responds only to the random energy of the forcing function centered about the resonant frequency of the structure. The principal response is essentially at the body's natural frequency, with contributions by more remote spectral components of the lift force being of minor order.

The first antenna installation (Winter Harbor, Maine) was an apparent effort to design the boom board as an aerodynamic shape (circular), but all subsequent designs reverted to a true bluff body shape (square or rectangular). The construction technique of the circular cross section at Winter Harbor was such that the cylinder was formed of two half circles bonded together through a one inch flange on

each side (Figure 2A). The flanges are located vertically one above the other, and produce distinct and unvarying flow separation points to the normal wind vector parallel to the ground. A typical rectangular boom board design is shown in Figure 2B. In this case the separation points are likely to occur at the corners.

It is the purpose of this paper first to investigate these oscillatory phenomena, specifically concerning the installation at Winter Harbor in an effort to theorize probable causes, and then to attempt to point out a reasonable "in the field" modification that might reduce oscillations to an acceptable level. It is also desired that the aeroelastic model and its associated equipment be usable for subsequent testing of shapes other than the cylinder.

These oscillations of bluff bodies have been observed since ancient times when the "Aeolian harp," or vibrating string principle, was noted. However, the underlying cause remained unknown until 1879, when Lord Rayleigh established that an unsteady lift force acting normal to the wind produced the motion. Much time and effort has been expended to fully explain these phenomena, but as yet the complete explanation of vortex shedding is still not clear. Von Karman published an article early in this century on the stability criteria required for steady spacing of trailing vorticies (sometimes called a vortex street), but his considerations did not relate to the mechanics of the vortex shedding phenomena. Familiar examples of these phenomena are: the hum or buzz of telephone wires; the vibration of structural smokestacks; the vibration of submarine periscopes; the sometimes violent motion of suspension bridges, such as the Tacoma Narrows Bridge (1940); and the launch limitations of present day missiles when exposed to groundwinds.

Concerning the antenna problem under consideration, some initial investigations have been undertaken by the United States Naval Civil Engineering Laboratory at Port Hueneme, California. These include an engineering study conducted by Simpson, Gumpertz, and Hager Inc. [7]. These investigations were primarily concerned with mechanical reactions, such as natural frequencies, structural damping, and resulting damage. Their results are summarized in Appendix A. Due primarily to the prohibitive size and locations of the individual antennas, the only sources of data for actual dynamic responses (amplitude and frequency) have been observations by personnel working on or around the antennas. These "on the site" observations indicate that boom board vibration starts at a wind velocity of about 30 knots, with rough estimation of frequencies on the order of six cycles per second. The magnitude of these vibrations increases with increased wind velocity.

The investigation reported in this paper relates to this problem from an aerodynamic viewpoint. It was conducted by the authors during the period of January through May, 1965 at the United States Naval Postgraduate School, Monterey, California. Sincere appreciation is extended to the faculty and staff of the Aeronautical Engineering Department for their assistance. The authors are deeply indebted to Professor L. V. Schmidt for his invaluable encouragement and assistance throughout the project.

2. Description of Model and Equipment.

The desired characteristics of a dynamic model for wind tunnel testing are quite stringent. Ideally the model would be very light weight, mounted on frictionless bearings, relatively immune to damgage from handling, able to reproduce desired frequencies, and sufficiently stiff so as not to introduce unwanted structural oscillations. In the problem under consideration, the general plan was to have the model hinged at one end with the other end free, and in this way provide a first approximation to one half of a boom board. Obviously the prototype boom boards have a mode shape that depends upon the installed end conditions and is functionally more complex. However, due to the long length of the boom boards and the end conditions close to simple supports, the first lateral vibration mode has been assumed to be dominant. This permits the aeroelastic model to be restricted to a single degree of freedom in the lateral direction.

Since it is required that the shape of the model be changeable for subsequent testing, it was decided to form the model of a center structure for strength, and some type of outer covering for the desired shape. It is also necessary that the lowest frequency of the model in the pinned-pinned mode be well above any frequency that might be encountered in testing, so that beat phenomena might be avoided. For this reason, an aluminum extruded "I" beam was chosen as the center structure. This beam, which extends the length of the model, has a natural frequency of 137 cycles per second, well above the maximum of about 100 cycles per second expected to be encountered in the experiment.

The outside shape of the model is reproduced by shaping middle grade balsa wood. The balsa is constructed in two halves, cut internally so

as to fit around the "I" beam (Figure 3A). It is held in place by tape wrapped around the model in a manner duplicating the wire hangers of the prototype boom boards, and by end plates which were fastened to the model "I" beam. The external balsa surface was finished with five coats of sanding sealer and eight coats of dope to present a smooth surface.

Instead of a normal hinge at the top of the model, a flexure plate was used in order to keep frictional damping small (Figure 3B). This flexure plate is clamped at the support structure and the model "I" beam, and allows motion primarily in the lateral direction. The size of the flexure plate was determined by considering the minimum length to accept a strain gage rosette, and the necessary width to support expected drag loading.

At the bottom of the model, a support is needed that will allow the model to vibrate, while providing the capability of varying the model's natural frequency, and still introduce a minimum amount of frictional damping into the system. The fixture chosen was a variable length "spring" bar cantilevered to the support structure and effectively pin connected to the model "I" beam. For ease of construction, as well as use, a drill steel rod, one half inch in diameter, was used. The cantilever support is a movable steel block, precision drilled to accept the spring bar and provided with four set screws which bind the spring bar in position. The block is then clamped to the relatively rigid base support structure (Figure 3C).

Connection of the spring bar to the model "I" beam is through a relatively frictionless pin joint. A cable arrangement (Figure 3D) transmits force through cable tension, but will transmit only a negligible twisting moment. The cable used was 1/16 inch by seven strand

stainless steel (breaking strength 500 pounds) instrument cable, which is considered quite flexible. The cable is under a tension preload as a result of adjustable plugs on each end. It is connected to the spring bar through a one quarter inch machine screw which screws into the rod, thus allowing easy removal. All joints of the cable are secured by silver solder. Model and support specifications are presented in Appendix F.

The wind tunnel utilized in this investigation is the 42 inch by 60 inch subsonic tunnel located in Building 234 at the United States Naval Postgraduate School, Monterey, California. This tunnel is a closed section, vertical return, 200 mile per hour installation by West Coast Research Corporation of Los Angeles, California. Power is supplied by two 150 horsepower electric motors driving two independent constant speed, variable pitch fans. Because no previous tests had been run in this tunnel, a test section pressure survey was made. The results of this survey are presented in Appendix B. The dynamic model was positioned vertically in the test section as shown in Figure 4.

Primary instrumentation for response measurement was either of two accelerometers located at the bottom of the model "I" beam. It was decided to measure acceleration instead of displacement because of the relative simplicity of installation and the reliability of an accelerometer, as compared with that of an inductance displacement measuring device. The two accelerometers employed were an Endevco type 2224B, and a Gulton type A321, both with a flat response curve to above 3000 cycles per second. After comparison of results on initial model tests, the Endevco accelerometer was selected as the primary data source, with back up provided by the Gulton. Calibration results of the Endevco

accelerometer are presented in Appendix C.

A secondary source of model response data was a pair of resistance strain gage rosettes located on the flexure plate. These gages were monitored during the tests, but no quantitative data was recorded.

Accelerations were recorded on a Brush Electronics Co. ink oscillograph and also observed on a Textronic type 545A cathode ray oscilloscope. A Ballantine "True RMS" voltmeter was used to obtain the root-mean-square values of the acceleration.

A block diagram of the instrumentation system is presented in Figure 5.

3. Model Scaling.

When scaling a dynamic model for wind tunnel testing, the variables which must be considered are: fluid density and viscosity; fluid velocity; model vibration frequency; and model inertia effects (stiffness, mode shapes, mass distribution, etc.). In low velocity flow problems, the fluid may be considered incompressible and Mach number effects neglected.

As has been stated, the first lateral vibration mode of the prototype boom boards has been assumed to be dominant, permitting the aeroelastic model to be restricted to one degree of freedom in the lateral direction. This allows the simplification that model inertia effects need not be scaled with respect to the prototype. The remaining variables combine into the dimensionless parameters: Reynolds number ($R = Vd/\nu$) and Strouhal number ($S = fd/V$).

Matching of Reynolds number between prototype and model assures that the aerodynamic forcing functions, which cause the vibrations, correspond. The estimated prototype Reynolds number, for large amplitude

response, varies from 250,000 to 750,000. In the flow about a circular cylinder, this is in the supercritical region where the RMS value of the unsteady lift force has been shown to be relatively constant. [5,6]. Thus, matching of Reynolds number will effectively occur, as far as dynamic model response is concerned, when the air flow about the model is supercritical. In order to convey a feeling of the magnitudes involved with respect to the test model, the variation of velocity and Reynolds number is presented as a function of dynamic pressure in Figure B-2.

Matching of the Strouhal number, or dimensionless frequency, assures dynamic response correspondence between prototype and model. [8]. The observations made at the Winter Harbor antenna, of large amplitude vibrations commencing at a wind velocity around 30 knots and having a frequency of about six cycles per second, indicate an initial Strouhal number of 0.2. Observations of the boom board vibrations at higher wind velocities do not include response frequency estimates, so it is not known how the prototype Strouhal number varies with velocity. If the boom boards react as normal bluff bodies - that is, essentially at their natural frequency - the response Strouhal number would decrease with increasing wind velocity.

4. Test Procedures.

To determine the system damping, and to calibrate the spring bar length as a function of the natural frequency of the model, a series of static tests was made with the wind tunnel inoperative. The model was mechanically displaced from the centered equilibrium position and then released, with the model's decaying response recorded on the Brush oscillograph. These tests were conducted from a spring bar length of 11-1/2 inches to three inches, in one half inch steps, and then repeated

to verify results.

Dynamic tests were conducted with the model in four configurations (Figure 6):

A - Smooth cylinder (no flanges), spring end clamped;

B - Smooth cylinder (no flanges), oscillating;

C - Cylinder with flanges at $\theta = \pm 90^{o}$, oscillating;

D - Cylinder with flanges at front and rear stagnation points, oscillating.

In the first dynamic test, the base pressure coefficient of the cylinder in configuration A was obtained over the full range of tunnel velocity. A pressure probe was positioned at the rear stagnation point as shown in Figure 7, with a micro-manometer being used to measure the difference in base pressure and reference static pressure.

The vibrational response of the model was obtained in a series of tests with the model in configurations B and C. Each test was run at a fixed natural frequency, set by positioning the calibrated spring bar to the proper length, while varying tunnel dynamic pressure. Before each test, a recheck of the model natural frequency was made in the same manner as in the static tests. Natural frequencies of 20, 30, 40, and 50 cycles per second were used for both configurations. The model's dynamic response, in the form of acceleration, was recorded on the Brush oscillograph, and the RMS values read from the Ballantine voltmeter. Visual observations, using the Textronic oscilloscope, were made of the response waveform in order to provide estimates and cross-checks of the frequency and acceleration values.

A final dynamic response test was conducted with the model in configuration D, and the spring bar set for a natural frequency of 20

cycles per second. Response data, as a function of tunnel dynamic pressure, was obtained in the same manner as previously indicated.

5. Results.

The principal results of this experiment are presented graphically in Figures 8 through 13. Appendix E contains tabular test data and results, and sample Brush oscillograms.

The static tests were conducted first to determine the system damping. When a lightly damped model is displaced from its equilibrium position and released, it will exhibit a decaying oscillation at the system's natural frequency. Typical of such a curve is Figure 8, which is the Brush oscillogram of the static test with a spring bar length of ten inches. All other static tests produced the same general picture, but at different natural frequencies. The damping ratio was determined from these oscillograms by use of the standard log decrement procedure. [2]. The average value of damping ratio computed from the static tests is 0.0183, indicating very light viscous and structural damping as expected. This value was determined from the results obtained with the model natural frequency below 30 cycles per second, where the damping ratios were well defined. Above 30 cycles per second the envelopes of the decaying oscillations are not quite so clear, but a damping ratio on the order of two per cent is still indicated.

The second purpose of the static tests was to calibrate the spring bar length as a function of the natural frequency of the model. The natural frequency for each static test was determined from the Brush oscillogram of the decaying oscillations. An attempt was made to predict this calibration using an engineering analysis based on an assumed harmonic aerodynamic forcing function acting at the model's

natural frequency. The results obtained from this analysis were quite different from the actual calibration obtained. This difference between measured and predicted system natural frequencies may be attributed to unknown elastic effects such as the support frame not being infinitely rigid, especially since the measured frequencies were lower than the predicted values. Regardless, the observed frequencies were repeatable, and therefore the curve of these frequencies with spring bar length (Figure 9) is used as the basis for determining model natural frequency. For practical use, it appears that the model should not be used above 50 cycles per second. At this point the curve commences a very steep gradient, making the natural frequency prohibitively sensitive to spring bar length.

In order to match aerodynamic forcing functions between prototype and model, tunnel flow must be set such that the model is operating at supercritical Reynolds numbers. In order to assure that the model Reynolds numbers were supercritical, the base pressure of the smooth cylinder (configuration A) was used as a criterion. The coefficient of base pressure, measured in the vicinity of the rear stagnation point, follows the same pattern with Reynolds number as the coefficient of drag. This was shown by Roshko from average pressure measurements over 20 or 30 degrees on either side of the rearmost point on a circular cylinder. [4]. Roshko found that the coefficient of base pressure had a value of about -1.0 at a Reynolds number of 100,000 and that at the transition to turbulent (supercritical) flow it dropped abruptly to about -0.2, then rose slowly in the supercritical range. Figure 10 shows the same general trend, but with slightly higher values of base pressure coefficient, which establishes supercritical flow at about a

Reynolds number of 200,000 (q = 10psf) and above. The difference between the base pressure values of Roshko and those measured here may be partially due to differences in the models; i.e., leakage around the ends of the cylinder, and surface roughness conditions. The ability to produce this supercritical flow at such a low value of dynamic pressure may be attributed to the tunnel turbulence level and the model surface roughness.

The RMS value of the unsteady lift force is essentially constant in supercritical flow. [5,6]. Thus, the aerodynamic forcing function of the prototype is matched on the model with tunnel dynamic pressure above ten pounds per square foot.

The dynamic tests of configuration B (smooth cylinder) were conducted at four degrees of model stiffness, represented by natural frequencies of 20, 30, 40, and 50 cycles per second. A typical response oscillogram is presented in Figure 11. The acceleration exhibits random amplitude fluctuations, with the frequency spectrum closely centered about the system's natural frequency. This agrees with the band-pass filter concept for supercritical flow about a bluff body developed in Appendix D. The plots of RMS acceleration in Figure 14 follow essentially the same curve for all values of natural frequency tested, increasing with dynamic pressure. These acceleration values are slightly lower (maximum of about two g's), but of the same order of magnitude as predicted in Appendix D. This correlation with unsteady aerodynamics theory confirms that the system design is functionally correct for this series of tests.

For the model in the prototype configuration C, there is no adequate theory available for response predictions. Prior investigations of the

dynamic response of a cylinder have dealt with the condition where the flow separation points are free to move over the surface of the cylinder. However, configuration C presents an entirely different problem, in that the separation points, at all flow velocities, are fixed at the flange positions ($\theta = \pm 90^{o}$). From this test it is seen that the RMS accelerations follow the same general trend as for configuration B, increasing with dynamic pressure and having approximately the same values regardless of model stiffness. However, the values of these RMS accelerations are up to six times higher (maximum of about 12 g's) than those of configuration B. Figure 14 compares the magnitudes of the response of the two configurations.

It is of interest to note that the maximum tunnel dynamic pressure attainable, with the model in configuration C, was 70 pounds per square foot. This is in comparison to a maximum of 100 pounds per square foot with the model tested in configuration B. This indicates that the more violent response of the flanged model extracts much more energy from the air flow than in the case of the smooth model. Thus, the higher frequency oscillations effectively increase the coefficient of drag of the model.

Contrary to the band-pass filter action of the smooth cylinder, the model's response in configuration C occurs at essentially a constant Strouhal number of about 0.17. Figure 15 shows the linear relationship between velocity and response frequency regardless of model natural frequency. Figure 12 is a Brush oscillogram of a configuration C test, which shows the harmonic nature of the response typical in all the tests of this model configuration. The constant Strouhal number of 0.17 is in reasonable agreement with the value of 0.2 estimated from

the "on the site" observations at the Winter Harbor antenna.

Investigating the response curves of configurations B and C in Figure 14, it is apparent that model stiffness has almost no effect on acceleration magnitudes. As has been stated, the smooth cylinder effectively reacts at its natural frequency, and it follows that the amplitude of motion is decreased by increasing natural frequency. This is in agreement with the harmonic relationship $a = \omega_N^2 y$, which is assumed to apply in general. However, the response of the model with flanges installed occurs at a constant Strouhal number, and is not dependent on model natural frequency. This effect was evident for all degrees of system stiffness. Therefore, an increase of the natural frequency of prototype configuration C has little effect on the amplitude of motion. Consequently, an increase in the natural frequency of the prototype installation would appear to have little effect on the amplitude of vibration, and does not seem to be an effective remedy for decreasing response.

Comparison of the tests made on configuration B and C indicate two distinct results which point to the effect of the flanges at $\theta = \pm 90^o$. First the magnitude of the response is increased greatly (approximately six times) by the addition of the flanges; and second, the frequency response changes from one of random nature, but with spectral components closely centered about the system's natural frequency, to one of harmonic nature at constant Strouhal number. It is apparent that the randomly oriented separation points of the smooth cylinder are associated with a wider distribution of spectral energy, and hence the structure response level is lower. The shedding of vortices from the flanges of the prototype configuration evidently occurs at a definite frequency proportional

to the flow velocity. Thus the aerodynamic forcing function has energy concentrated near to a constant Strouhal number, and the structure has no choice but to respond at a frequency corresponding to that Strouhal number.

Extending the results of this analysis to the prototype boom board, it is obvious that any "in the field" solution to the vibration problem will require modification of the external flanges. Since these flanges are necessary for structural assembly, they cannot be removed. Suitable shrouding could possibly be installed around the flanges that would allow the air flow to pass the 90 degree position without separating. A more simple modification would be possible if the Winter Harbor installation is such that the boom boards could be rotated 90 degrees about their longitudinal axes. This would place the flanges at the front and rear stagnation points, and should have the effect of matching the dynamic response to that of a smooth cylinder.

This "fix" is represented by configuration D, which was tested at a model natural frequency of 20 cycles per second. Figure 14A presents a comparison of the responses of the three configurations tested at this frequency. The RMS acceleration values of configuration D are almost identical to those of configuration B, reaching a somewhat smaller peak value of 1.6 g's. This represents a decrease in magnitude by a factor of about six from the response of the prototype configuration C. The Brush oscillogram of Figure 13 indicates that the response frequency is again random natured, centered about the model's natural frequency. Therefore, it is considered that the modification represented by configuration D would be a satisfactory aerodynamic solution to the problem of reducing the amplitude of boom board vibration at the Winter Harbor

antenna site.

6. Conclusions.

Air flow over a circular cylinder with flanges 90 degrees from the front and rear stagnation points, such as the boom boards in the Winter Harbor, Maine antenna installation, is characterized by periodic vortex shedding at the separation points defined by these flanges. The dynamic response of such a cylinder occurs at a constant Strouhal number, with random amplitude significantly greater in RMS value than that of a smooth cylinder. In this experiment the flanged model responded at a Strouhal number of 0.17, with RMS acceleration values approximately six times greater than the corresponding response of the smooth model.

An aerodynamic solution to the problem of large amplitude vibrations of the Winter Harbor boom boards is rotation of these boom boards 90 degrees, so that the flanges are positioned at the front and rear stagnation points relative to the normal wind vector parallel to the ground. Dynamic response to flow over a cylinder with the flanges in this position is essentially the same as in the case of a smooth cylinder. This "in the field" modification would reduce the amplitude of vibration substantially.

It is recommended that subsequent testing include a hot-wire wake survey for the prototype configuration to confirm the existence of periodic vortex shedding in the supercritical flow range.

BIBLIOGRAPHY

1. Fung, Y. C. An Introduction to the Theory of Aeroelasticity. John Wiley and Sons, 1955.

2. Scanlon, R. H. and Rosenbaum, R. Introduction to the Study of Aircraft Vibration and Flutter. MacMillan, 1951.

3. Thomson, W. T. and Barton, M. V. The Response of Mechanical Systems to Random Excitation. Journal of Applied Mechanics, v. 24, no. 2, June, 1957: 248-251.

4. Roshko, A. Experiments on the Flow Past a Circular Cylinder at Very High Reynolds Number. Journal of Fluid Mechanics, v. 10, part 3, 1961: 345-356.

5. Space Technology Laboratories, Ramo-Wooldridge Corporation. Fluctuating Lift and Drag Acting on a Cylinder in a Flow at Supercritical Reynolds Numbers, by Y. C. Fung. 7 May 1958. Technical Report GM-TR-0165-00343.

6. Space Technology Laboratories, Ramo-Wooldridge Corporation. The Analysis of Wind-Induced Oscillations of Large and Tall Cylindrical Structures, by Y. C. Fung. June, 1960. Technical Report STL/TR-60-0000-09134.

7. District Public Works Office, First Naval District, Boston, Massachusetts. Effect of Wind-Induced Vibrations on the Structural Integrity of Fiberglass Reinforced Plastic Booms, by Simpson, Gumpertz, and Heger Inc. March, 1964. Engineering Service Contract 23(64).

8. Aerospace Corporation. Review of Dynamic Scaling for Ground Wind Load Models, by L. V. Schmidt. 22 June 1964. Technical Memorandum 64(4116-42)-2.

FIGURE 1
ANTENNA INSTALLATION
GENERAL LAYOUT

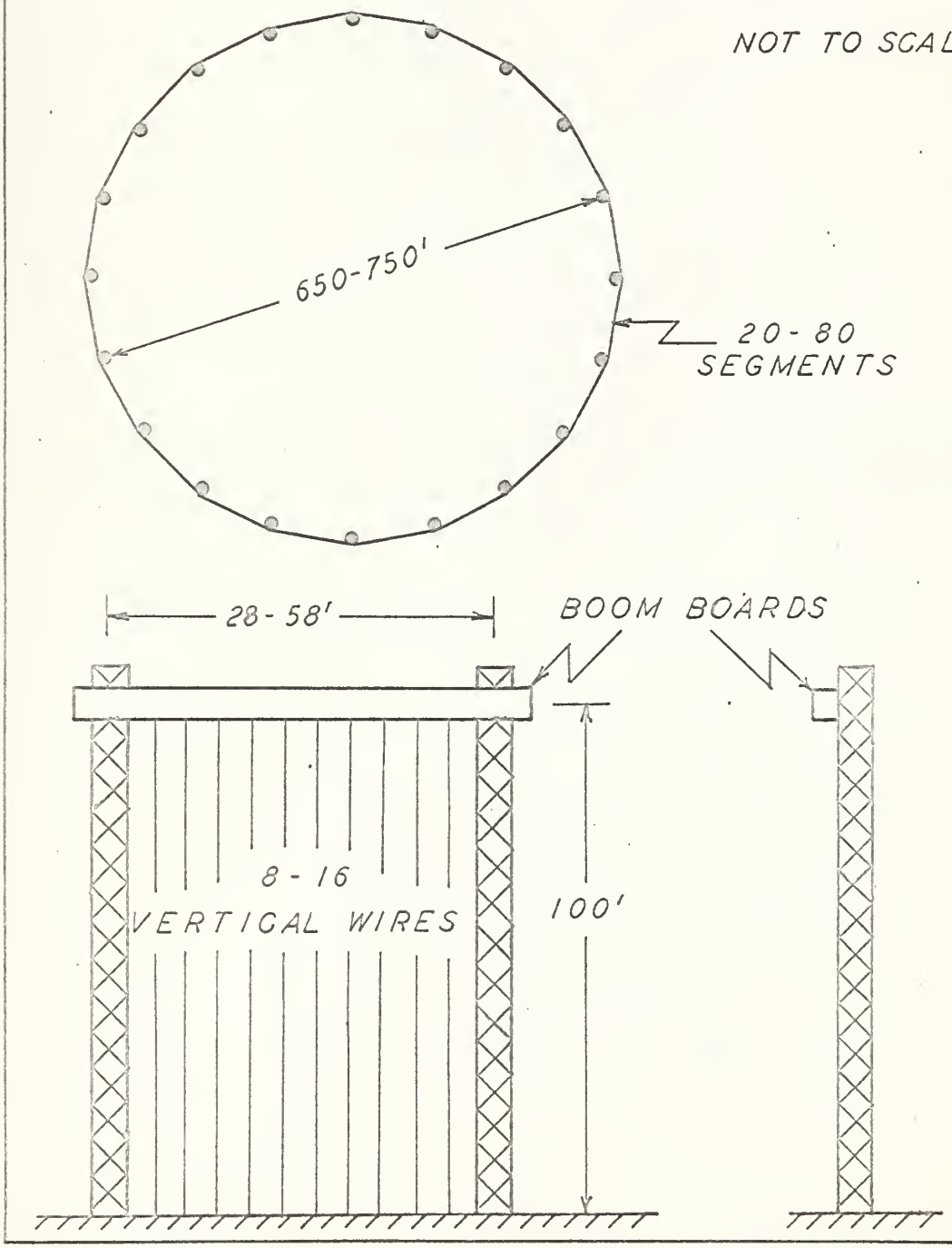

FIGURE 2A

CIRCULAR BOOM BOARD

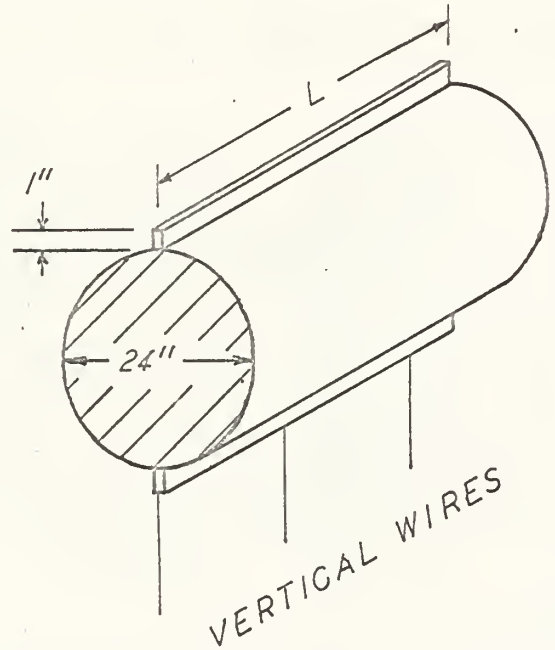

FIGURE 2B

RECTANGULAR BOOM BOARD

$1 \leq h:d \leq 2.48$

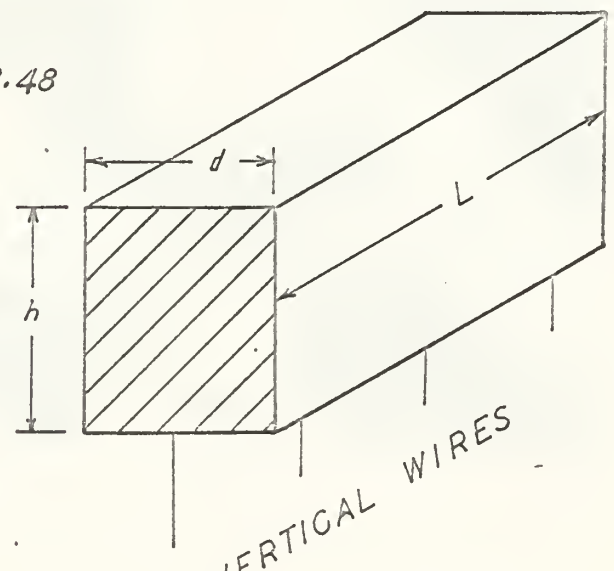

FIGURE 3A

SCHEMATIC OF MODEL ASSEMBLY

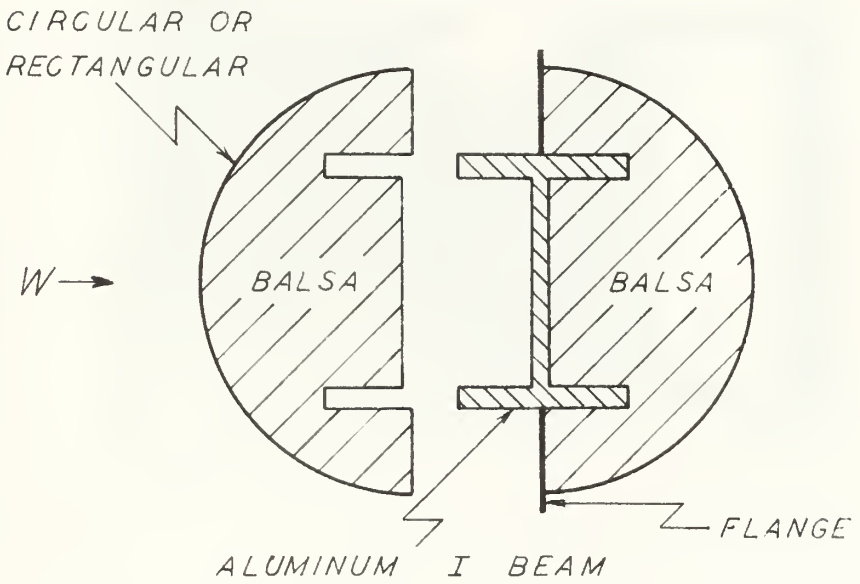

FIGURE 3B

FLEXURE PLATE

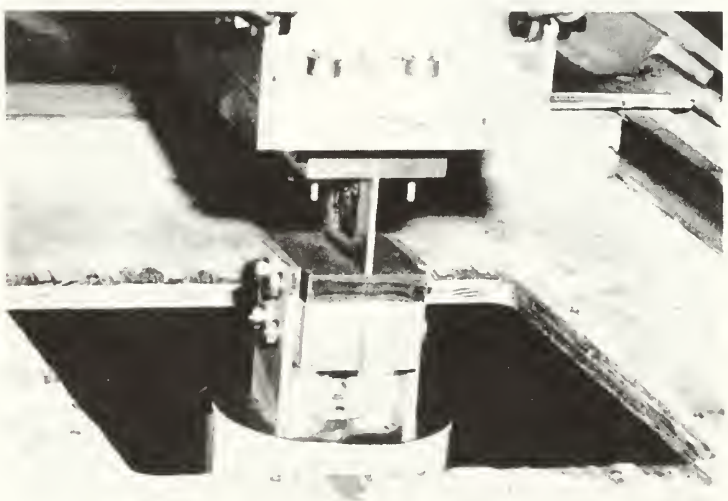

FIGURE 3C
ADJUSTABLE BLOCK

FIGURE 3D
SPRING BAR JOINT

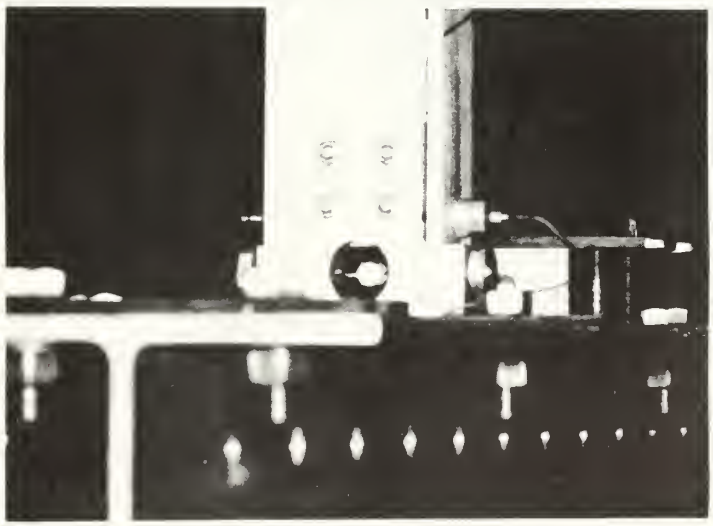

FIGURE 4
COMPLETE INSTALLATION

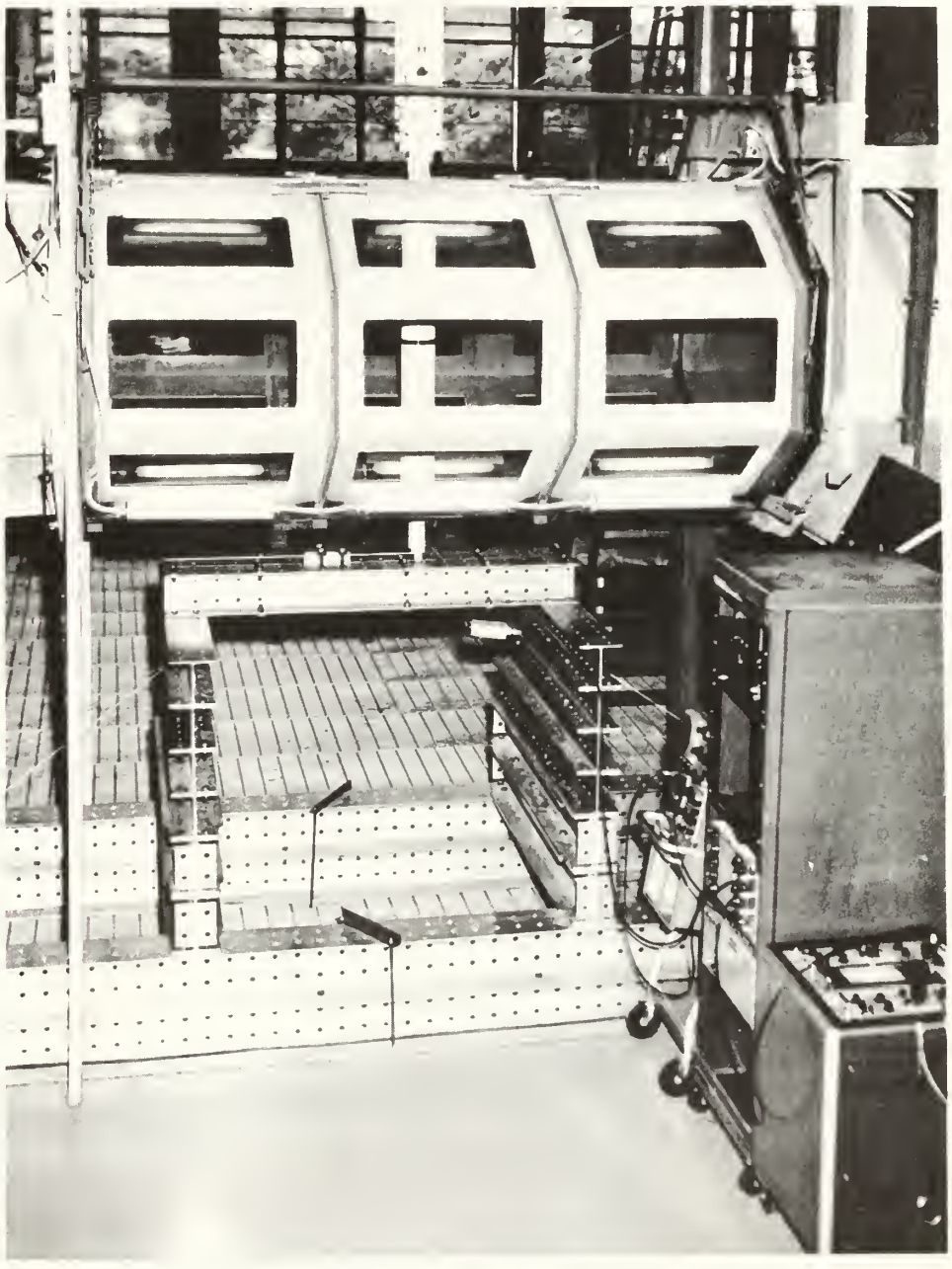

FIGURE 5
BLOCK DIAGRAM OF INSTRUMENTATION

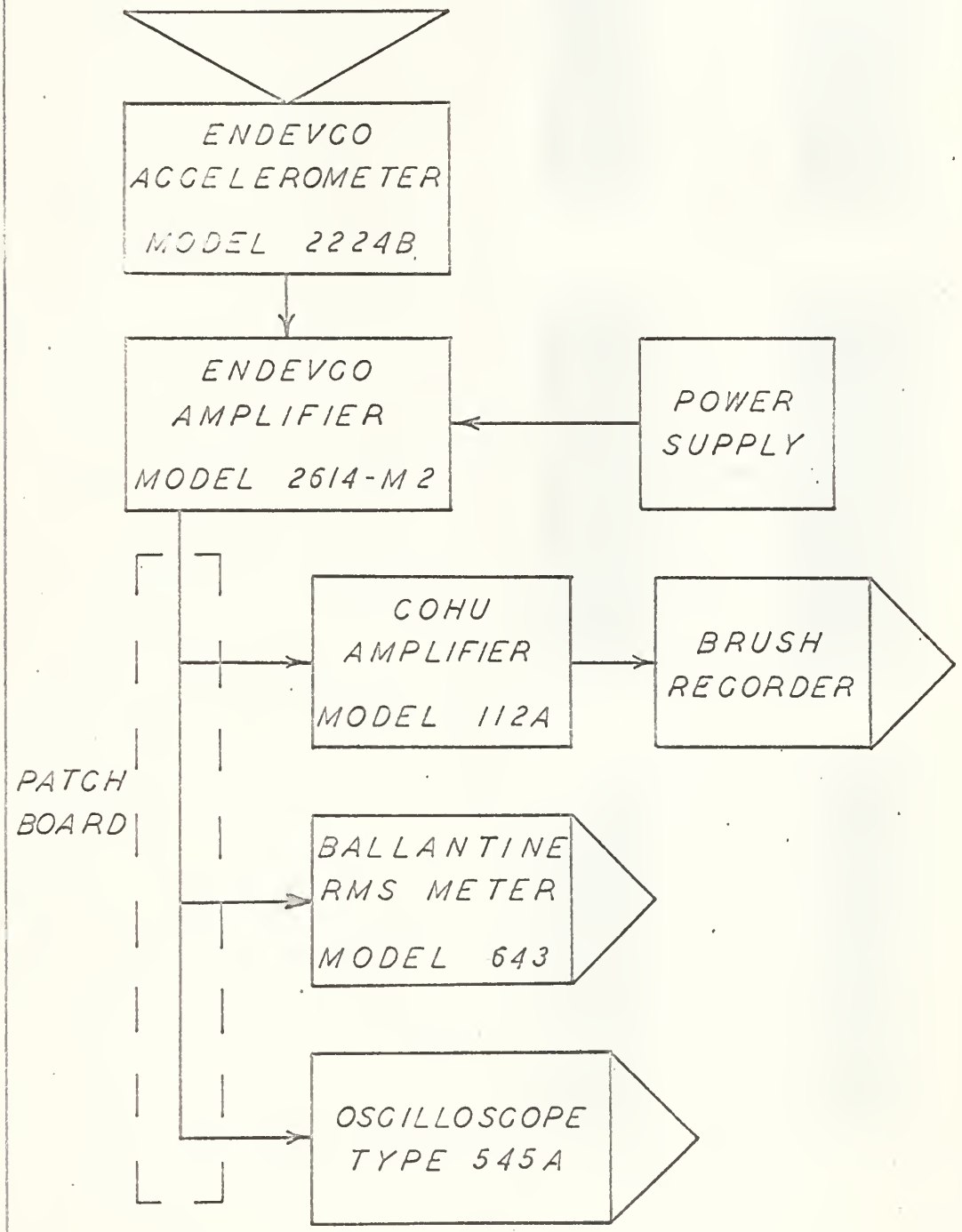

FIGURE 6A
CONFIGURATION B
SMOOTH CYLINDER

FIGURE 6B
CONFIGURATION C
FLANGES AT 90°

FIGURE 6C
CONFIGURATION D
FLANGES AT 0-180°

FIGURE 7

BASE PRESSURE PICKUP

FIGURE 8

BRUSH RECORDER TRACING OF STATIC TEST

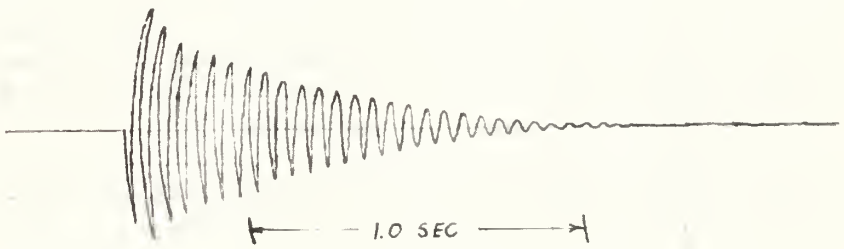

$\ell_B = 10.5''$ $f_N = 18.5$ cps $\beta = 0.0190$

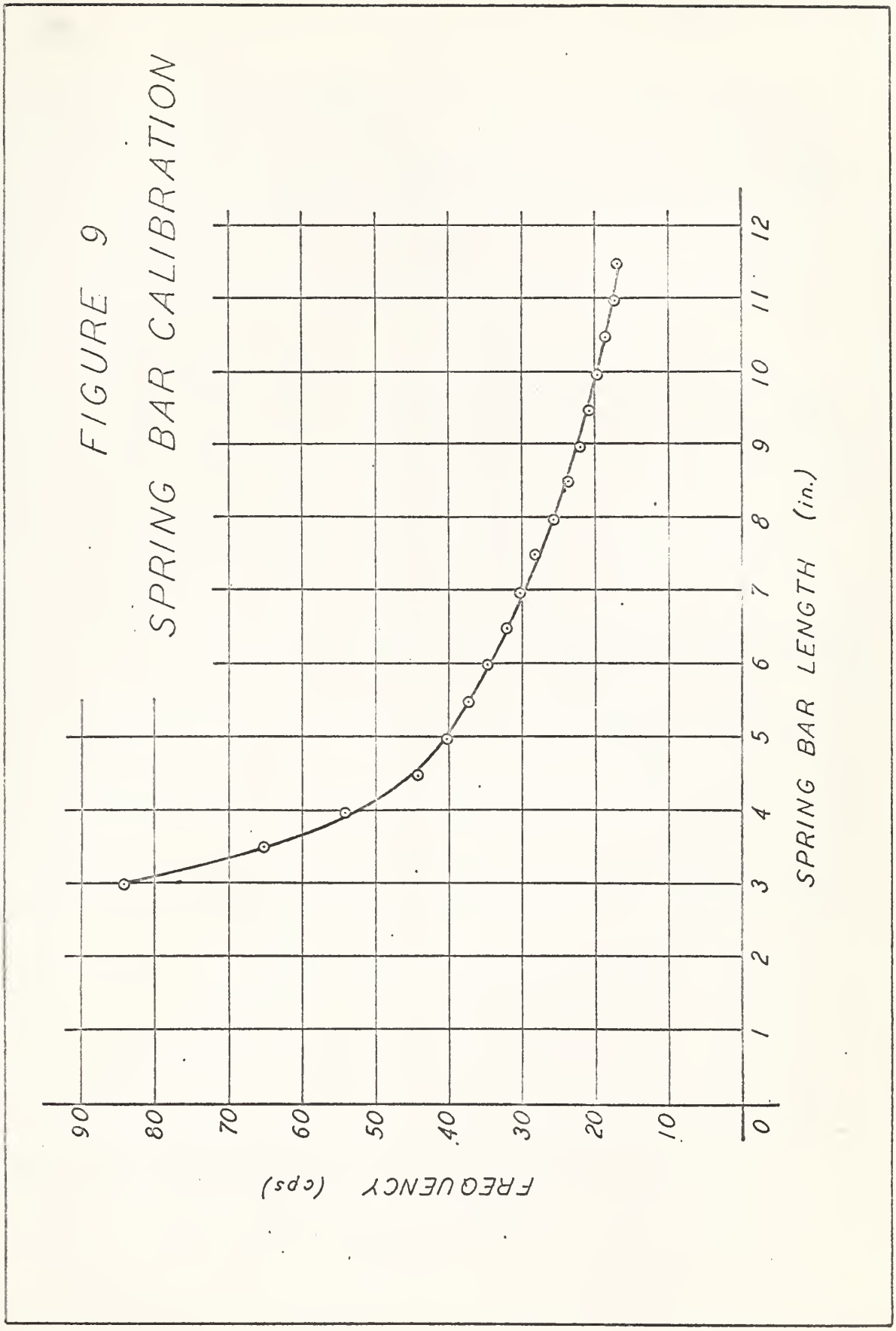
FIGURE 9
SPRING BAR CALIBRATION
FREQUENCY (cps)
90
80
70
60
50
40
30
20
10
0
1
2
3
4
5
6
7
8
9
10
11
12
SPRING BAR LENGTH (in.)

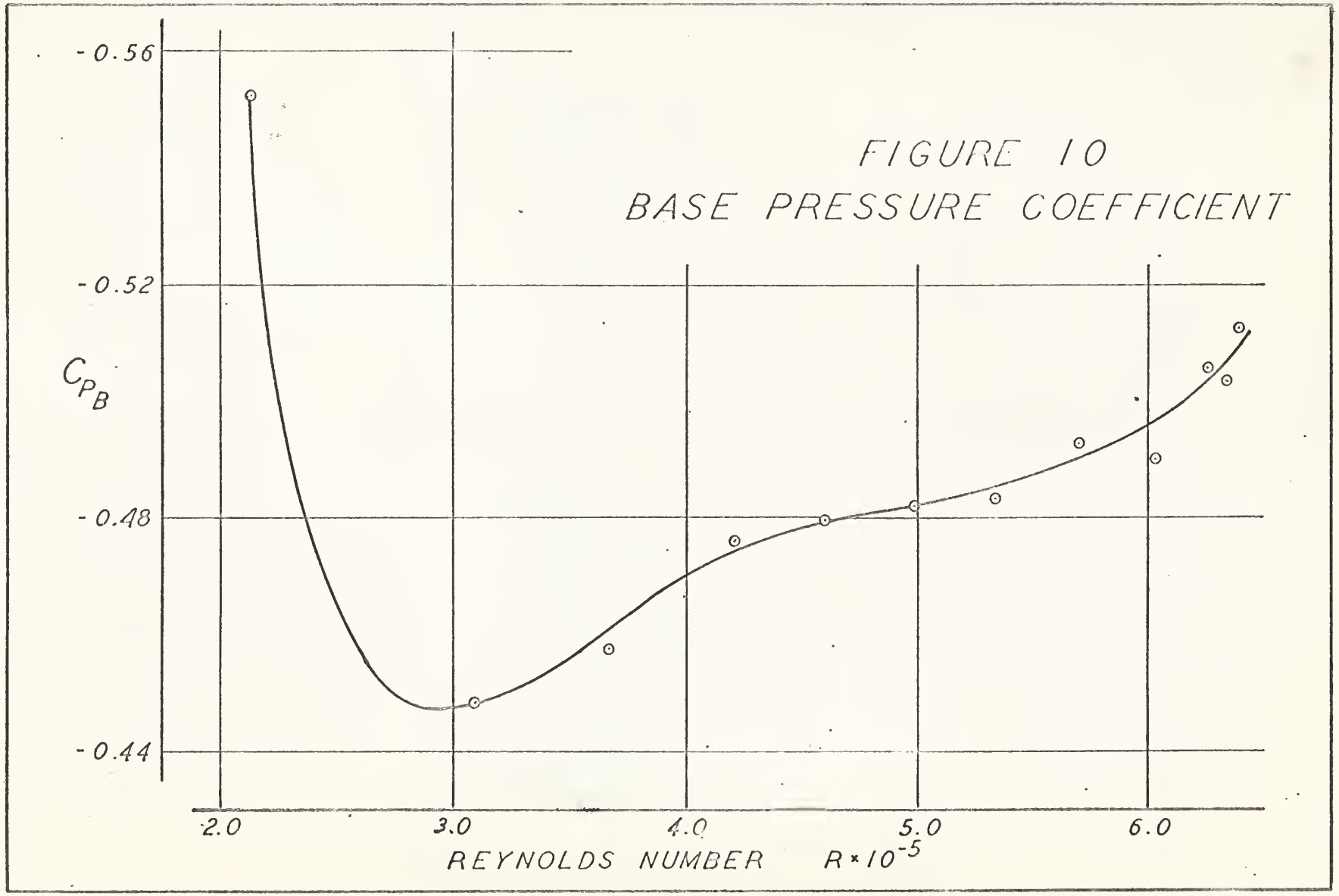
FIGURE 10
BASE PRESSURE COEFFICIENT
-0.56
-0.52
-0.48
-0.44
C_{P_B}
2.0
3.0
4.0
5.0
6.0
REYNOLDS NUMBER $R \times 10^{-5}$

FIGURE 11

OSCILLOGRAPH TRACE OF CONFIGURATION B

$f_N = 20$ cps $f_{AVE} = 25.6$ cps $q = 28.4$ #/ft² $\sqrt{\bar{a}^2} = 0.623$ g's

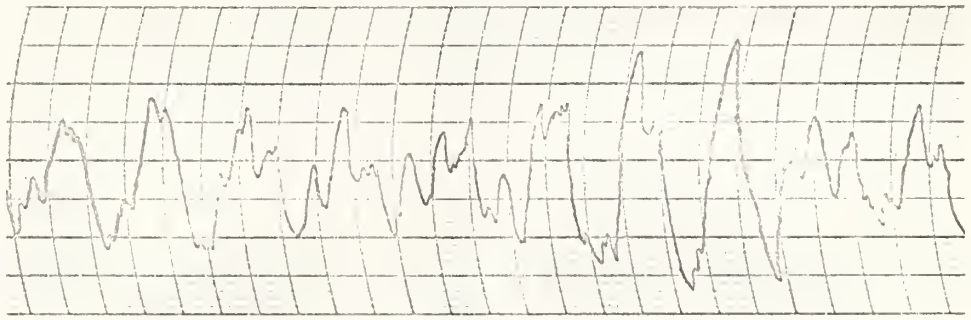

FIGURE 12

OSCILLOGRAPH TRACE OF CONFIGURATION C

$f_N = 20$ cps $f = 61$ cps $q = 29.0$ #/ft² $\sqrt{\bar{a}^2} = 4.42$ g's

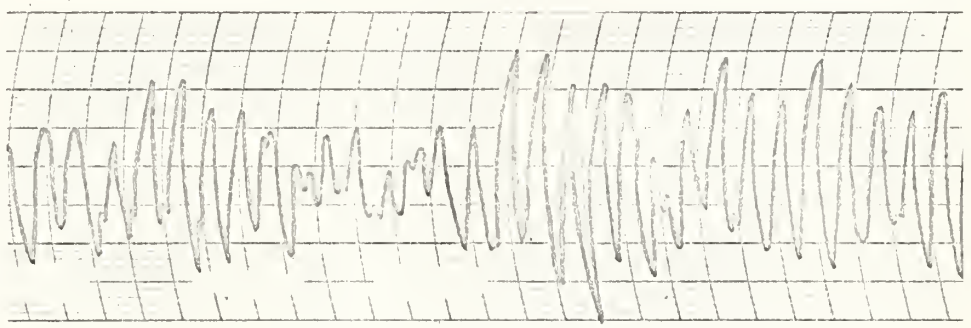

FIGURE 13

OSCILLOGRAPH TRACE OF CONFIGURATION D

$f_N = 20$ cps $f_{AVE} = 20.5$ cps $q = 27.05$ #/ft² $\sqrt{\bar{a}^2} = 0.554$ g's

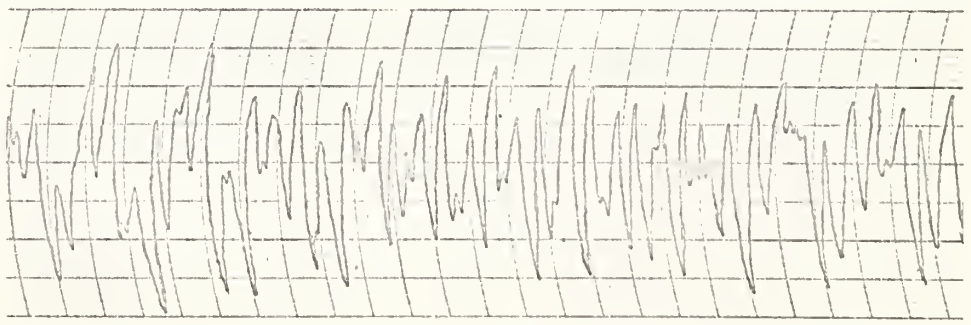

FIGURE 14A
DYNAMIC RESPONSE
CONFIGURATIONS B.C.D
f_N = 20 cps

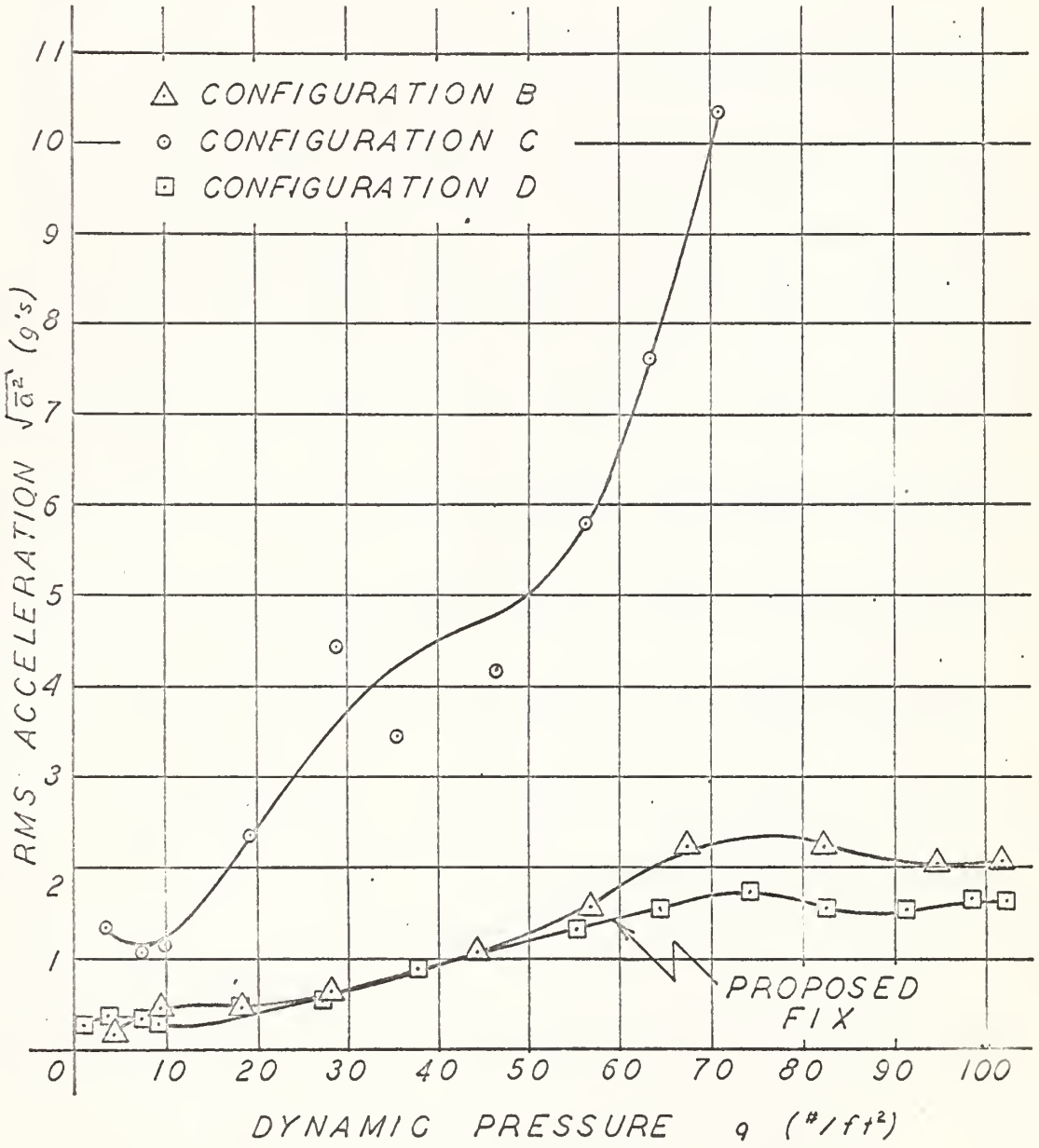

FIGURE 14B
DYNAMIC RESPONSE
CONFIGURATIONS B, C

f_N = 30 cps

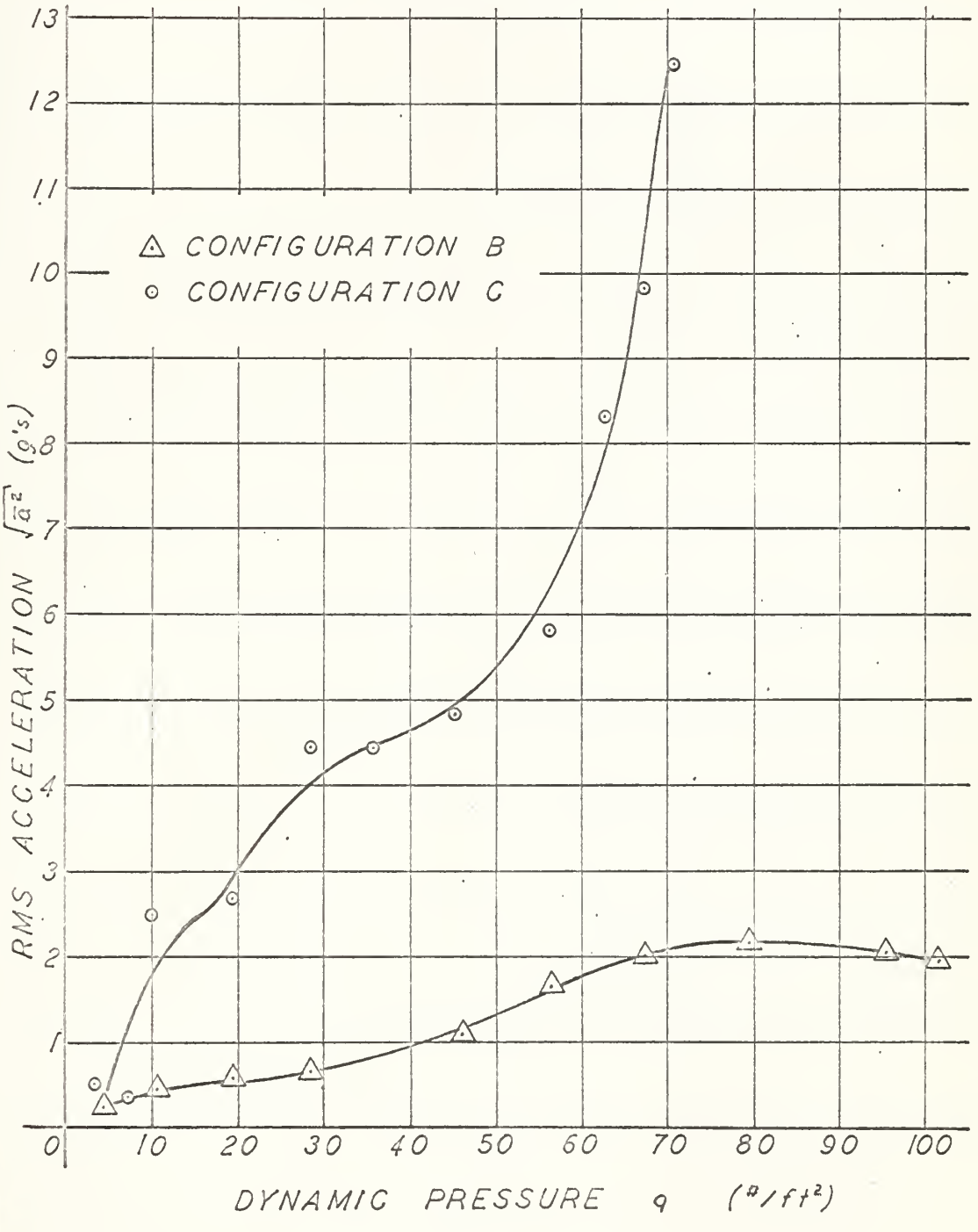

FIGURE 14C
DYNAMIC RESPONSE
CONFIGURATIONS B,C
f_N = 40 cps

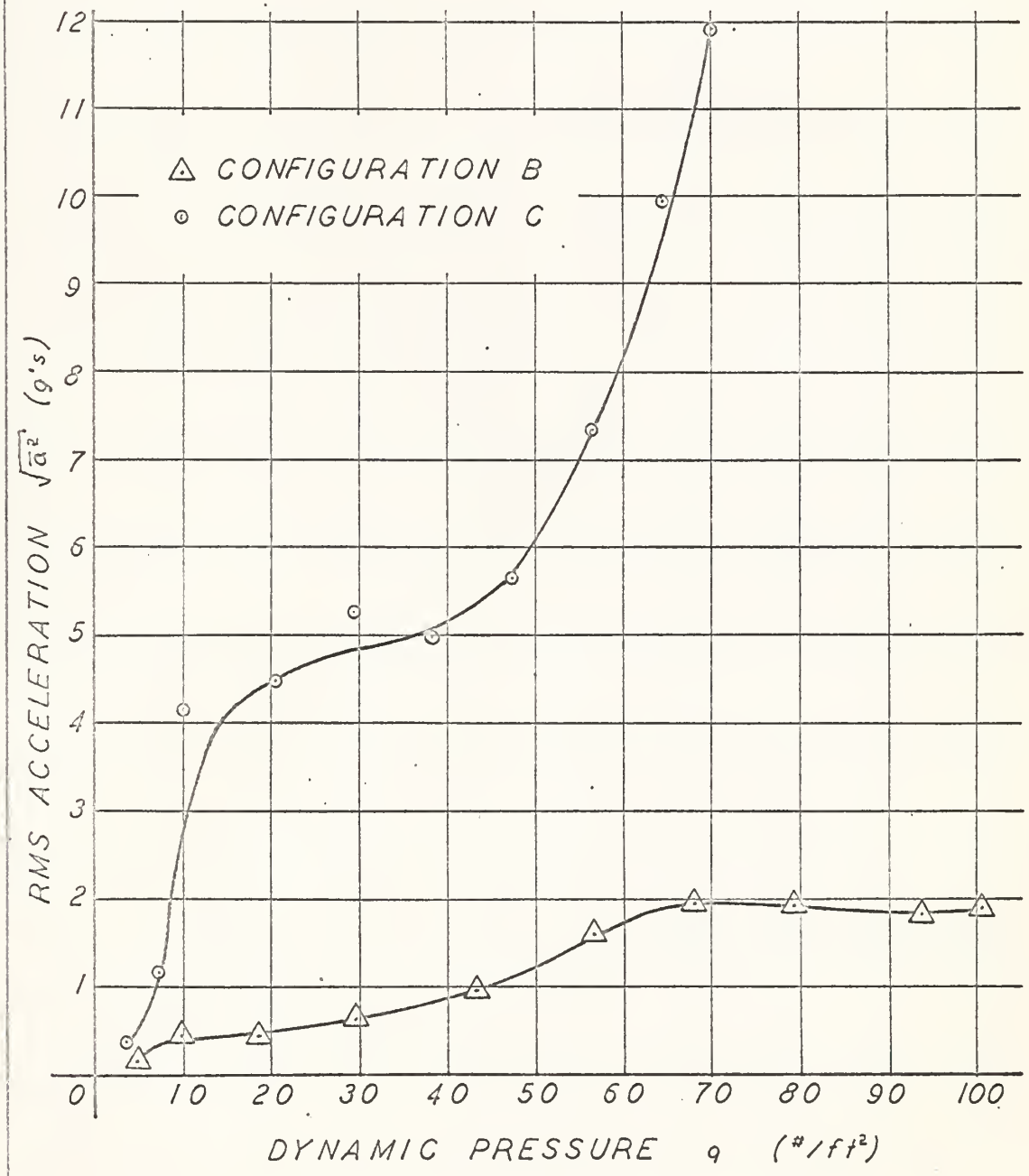

FIGURE 14D
DYNAMIC RESPONSE
CONFIGURATIONS B, C
f_N = 50 cps

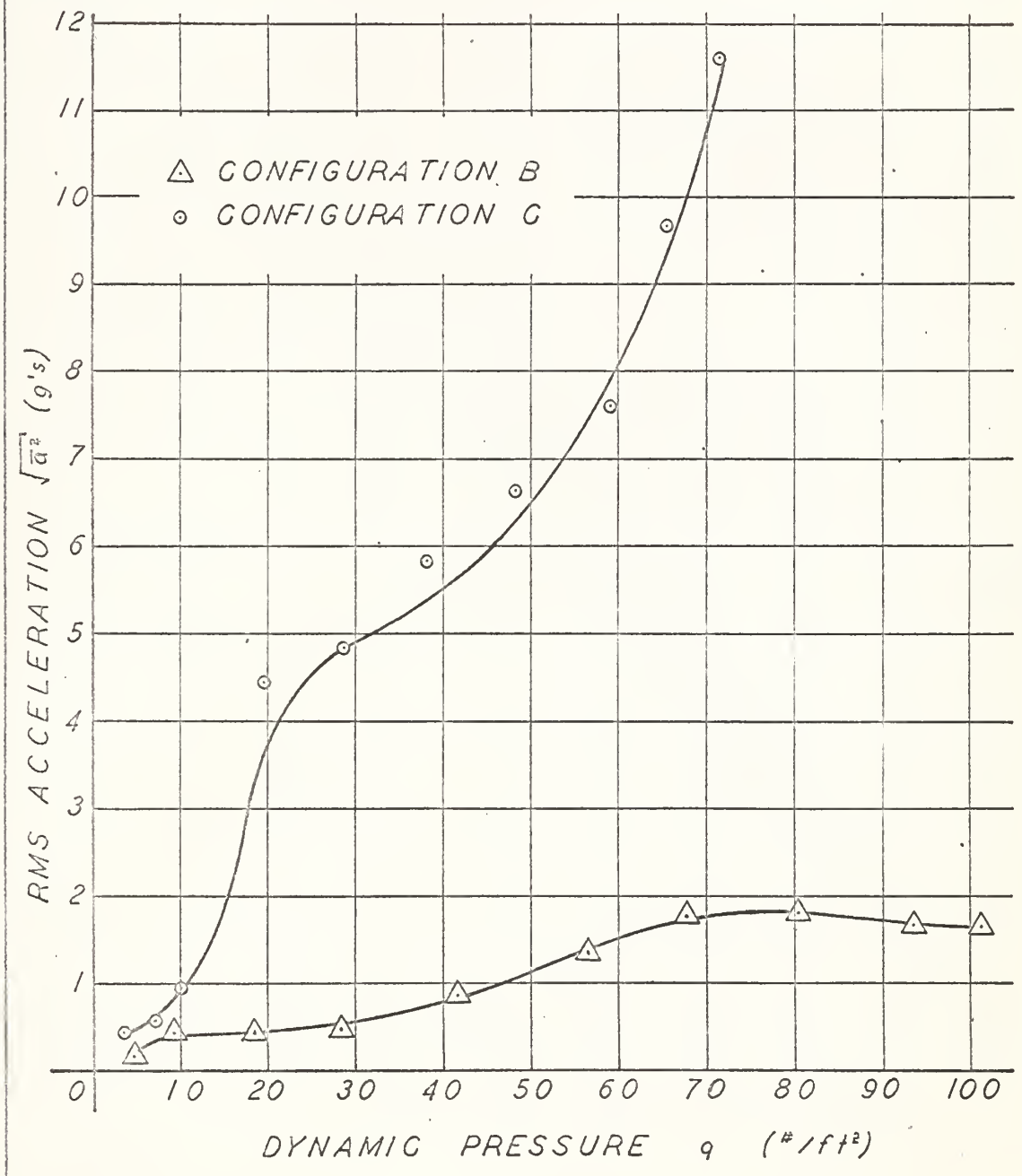

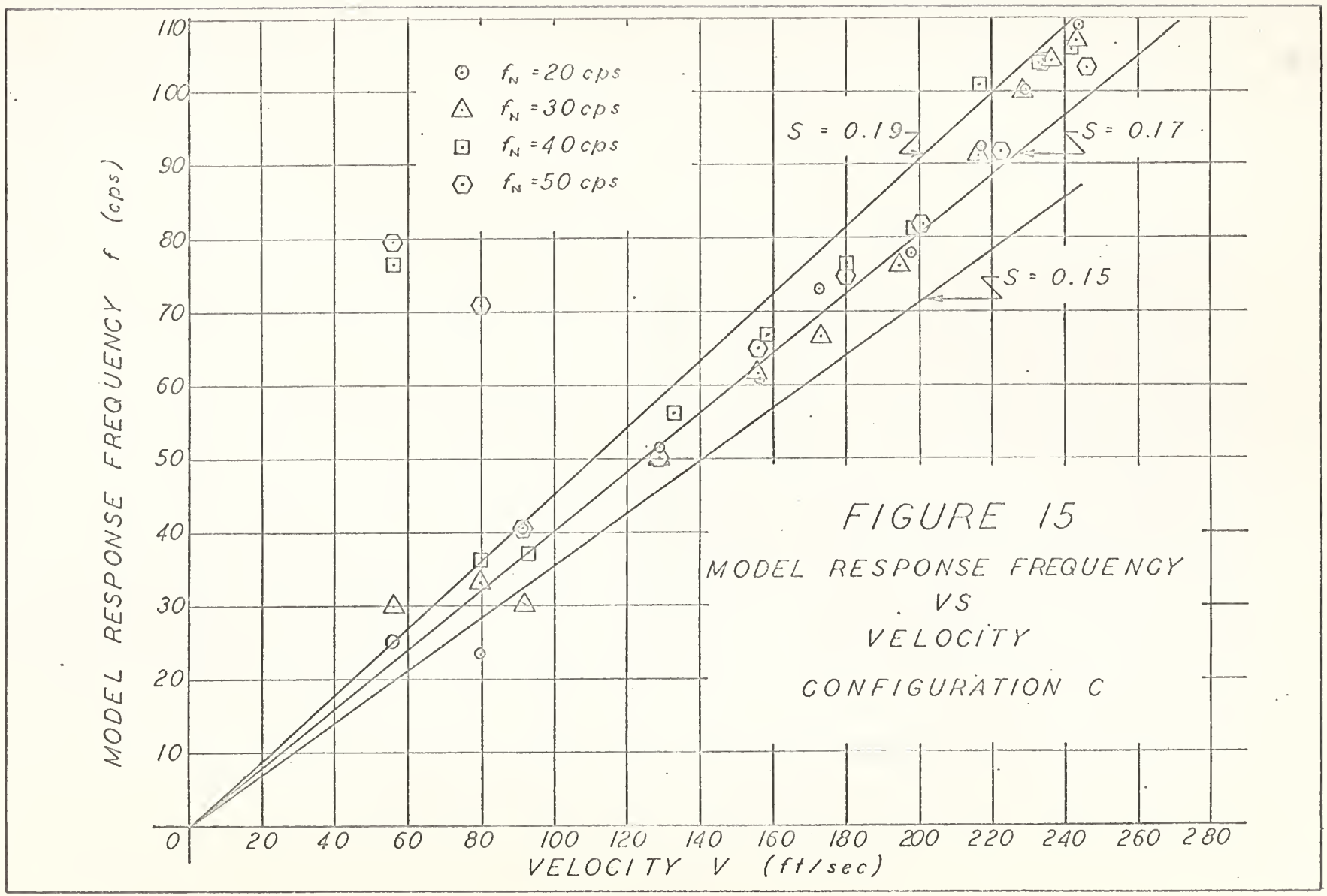

FIGURE 15

MODEL RESPONSE FREQUENCY VS VELOCITY

CONFIGURATION C

APPENDIX A

GENERAL ANTENNA INFORMATION

GENERAL ANTENNA SPECIFICATIONS

STATUS Mid-1964

Kadena, Okinawa f_N = 3.10 cps β = 0.351	BOOM-3 layer glass fabric over 3/4" plywood, approximately 45' span; BOOM SUPPORT-steel tower with boom hung from bracket (turnbuckle); SCREEN WIRE-#10 copper wire with turnbuckle at bottom; REMARKS-this array is different from standard-smaller diameter-higher screen 2 intermediate lateral supports for wires.
Guam f_N = 9.17 cps β = 0.312	BOOM-Wood, similar to Okinawa, approximately 28' span; BOOM SUPPORT-same as Okinawa; SCREEN WIRE-#8 solid copper wire with turnbuckle; REMARKS-1 intermediate lateral support for wires.
Honolulu f_N = 7.35 cps β = 0.349	BOOM-laminated wood (3-2x8"), approximately 28' span; BOOM SUPPORT-guyed wood poles hung from a yard arm, no lateral stays; SCREEN WIRE-#10 copper, connected through spring, 50# initial tension. 
Adak, Alaska f_N = 11.29 cps β = 0.236	BOOM-glued box section (4-2x8"), fiber glass outer surface, approximately 28'6" span; BOOM SUPPORT-guyed wood poles; SCREEN WIRE-#10 copperweld with turnbuckle and intermediate support 
Marietta, Washington NOWESTDIVDOCKS	Same as Adak
Skaggs Island, San Francisco 12th ND 	BOOM-glued inverted "U" section (3-2x8"), wires hung from individual 2x8's, 28'6" span; BOOM SUPPORT-guyed wood poles, boom is hung from yard arm with turnbuckle, no lateral stay; SCREEN WIRE-#10 copper encased with spring.
Imperial Beach, California	BOOM-laminated wood (5¼"x13") 5/8" camber, approximately 28'6" span; BOOM SUPPORT-guyed wood poles, boom seated on steel bracket, stayed laterally; SCREEN WIRE-#8 AWG, spring and turnbuckle.
Scotland, Edzell	BOOM-same as Skaggs Island; BOOM SUPPORT-guyed wood poles, boom hung from yard arm, turnbuckle attempts made to stay the lateral motion; SCREEN WIRE-#10 copper encased with springs
Sabana Seca, Puerto Rico	BOOM-glued inverted "U" section (3-4x14"), wires hung from individual 4"x14"x10", approximately 57' span; BOOM SUPPORT-guyed wood poles, boom seated on wood pole, fairly rigid connection; SCREEN WIRE-#10 noncorrosive copper with turnbuckles, 100# initial tension; REMARKS-contract let, but not yet built.

Galeta, Canal Zone	BOOM-glued inverted "U" section (3-4x12"), wires hung from individual 4"x12"x10", approximately 58' span; BOOM SUPPORT-guyed wood poles, boom seated on bracket on pole, fairly rigid; SCREEN WIRE-#10 copperweld with turnbuckle, 100# initial tension.
Northwest Virginia	BOOM-laminated wood (9"x13"), 57' span; BOOM SUPPORT-guyed wood poles, boom hung from yard arm; SCREEN WIRE-#10 copperweld with turnbuckles, 100# initial tension; REMARKS-two booms have failed due to poorly designed end connection, screen was designed for springs, but station was ordered to use turnbuckles, springs have since been requested by sponsor.
Winter Harbor, Maine f_N = 7.35 cps β = 0.235 	BOOM-24" circular reinforced plastic beam, 48' span, beam tapers near support to approximately 14" diameter; BOOM SUPPORT-steel tower, boom sits in saddle with the tie down straps on bracket of tower; SCREEN WIRE-spring mounted with 150# initial tension; REMARKS-vibrating boom breaks wires, stretches springs, breaks anchor bolts, and rotates boom in saddle.
Homestead, Florida	BOOM-glued wood box section (2-2x8" and 2-2x10"), approximately 28'6" span; BOOM SUPPORT-guyed wood poles, boom is supported on a seat bracketed from pole; SCREEN WIRE-0.165 H.S. 40o/o, turnbuckle and spring at base; REMARKS-in state between design and letting contract, end connection might give trouble.
Rota, Spain	BOOM-glued inverted "U" section (3-2x8"), wires hung from individual 2"x8", approximately 28'6" span; BOOM SUPPORT-guyed wood poles, boom is hung and stayed laterally with turnbuckles; SCREEN WIRE-#10 copper encased, spring and turnbuckle at base; REMARKS-construction under way.

FIGURE A-1

AIR PHOTOGRAPH OF
HONOLULU ANTENNA

APPENDIX B

WIND TUNNEL TEST SECTION CALIBRATION

APPENDIX B

WIND TUNNEL TEST SECTION CALIBRATION

The test section pressure survey shown in Figure B-1 was performed on the United States Naval Postgraduate School's low speed wind tunnel located in Building 234. Small shrouded total and static pressure probes were used for the vertical survey four feet from the test section leading edge. The reference dynamic pressure was measured at the test section leading edge. Based on this survey, the following calibration values were used:

$$\frac{q_{\text{test section}}}{q_{\text{reference}}} = 0.945;$$

$$\frac{P_{\text{static}} - P_{\text{atmospheric}}}{q_{\text{reference}}} = -0.08.$$

Average tunnel operating conditions in the form of velocity and Reynolds number for a five inch model are plotted against dynamic pressure in Figure B-2.

FIGURE B-1

PRESSURE SURVEY

USNPGS 3.5' × 5.0' WIND TUNNEL

q_{REF} = 87.8 psf (TEST SECTION LEADING EDGE)

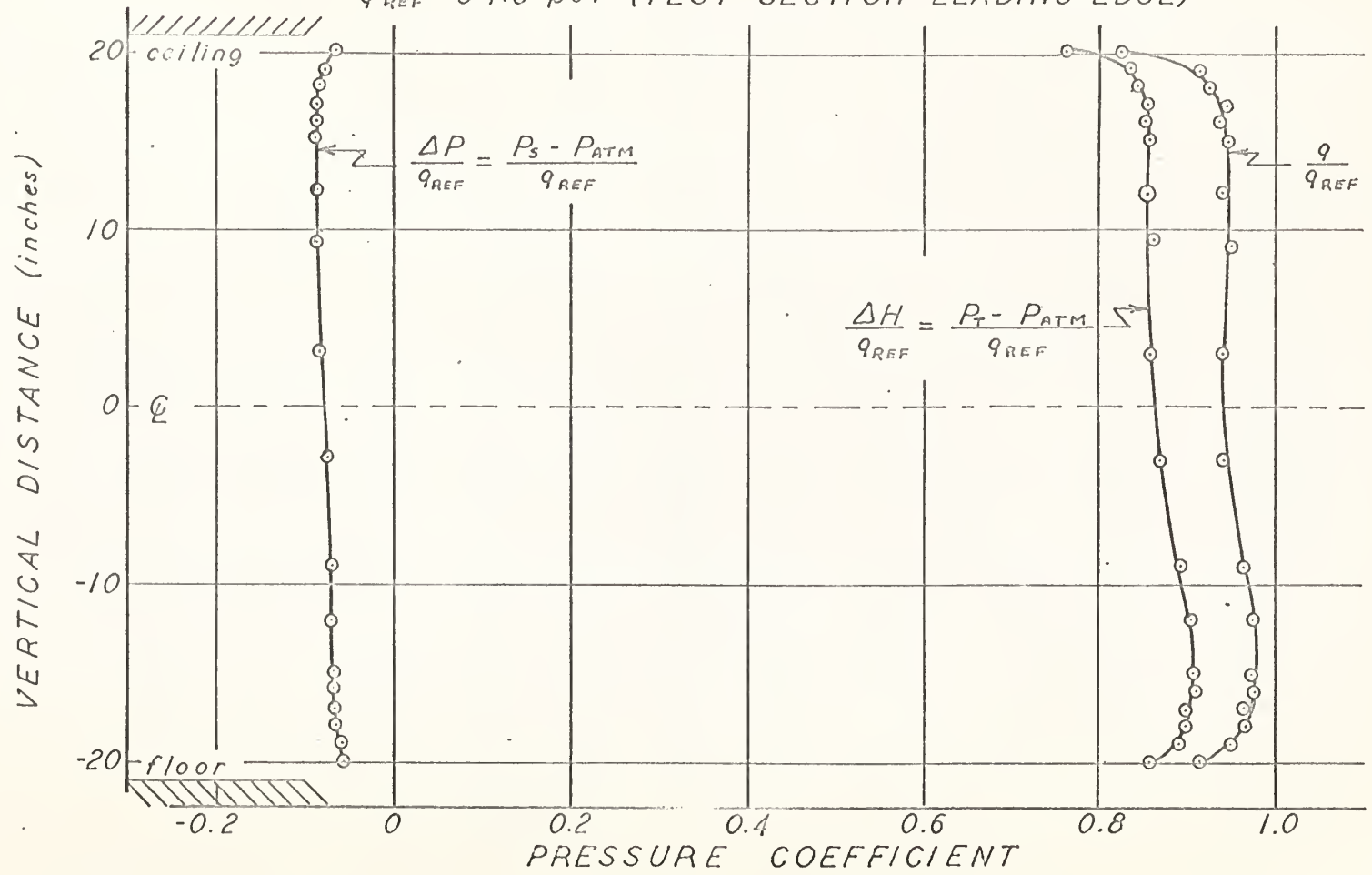

FIGURE B-2

WIND TUNNEL OPERATING CONDITIONS

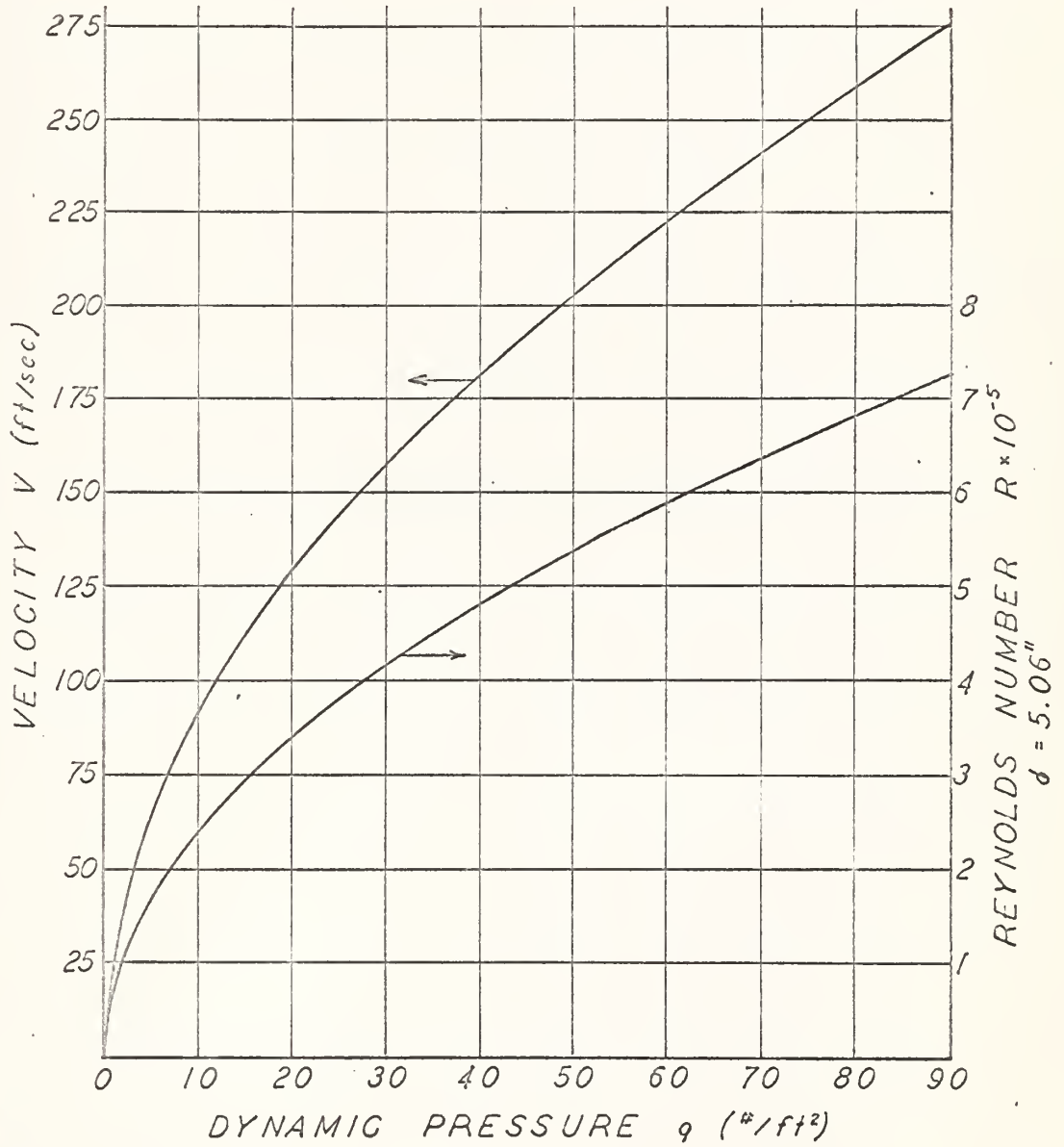

APPENDIX C

ACCELEROMETER CALIBRATION

APPENDIX C

ACCELEROMETER CALIBRATION

The accelerometer employed as the primary source of data was an Endevco type 2224B, Serial Number AA42. This accelerometer, coupled with an Endevco amplifier, was calibrated by harmonic excitation through a frequency range from 50 to 150 cycles per second on a Calidyne model A88 shaker table. Accelerations were calculated from a direct measurement of displacement using an electro-optical transducer, the Optron Displacement Follower, model 701, Serial Number 701-313.

Response was recorded up to a frequency of 150 cycles per second as indicated in Table C-I and plotted in Figure C-1. The calibration of the Endevco accelerometer taken from this graph is:

$$\frac{\text{RMS volts}}{\sqrt{\overline{a^2}}\ \text{(g's)}} = 0.0724.$$

TABLE C-I

Endevco Accelerometer Calibration

Accelerometer Serial #AA42
Endevco Amplifier Serial #AB54
Gain - 10x
Setting - #1
Capacitance - 780$\mu\mu$f

f (cps)	Phototron RMS volts	Displacement RMS (in)	$\sqrt{a^2}$ (g)	$\sqrt{a^2}$ (volts)
20	0.385	0.00570	0.234	0.0166
	0.755	.0112	.459	.0332
	1.12	.0167	.685	.050
	2.00	.0296	1.21	.105
	0.58	.00858	0.352	.0250
50	0.195	0.00288	0.739	0.0555
	.350	.00518	1.33	.0975
	.500	.00740	1.90	.134
	1.00	.0148	3.80	.282
	1.40	.0207	5.31	.420
	0.60	.00888	2.27	.159
101	0.080	0.00118	1.20	0.096
	.198	.00293	2.99	.240
	.317	.00469	4.78	.346
	.515	.00762	7.27	.542
	.240	.00352	3.59	.261
150	0.030	0.000444	1.02	0.0718
	.0712	.00105	2.42	.169
	.100	.00148	3.42	.237
	.201	.00298	6.86	.458
	.300	.00444	10.2	.680
	.140	.00207	4.78	.321

Optron Calibration 0.0148 in/v

FIGURE C-1

ENDEVCO ACCELEROMETER CALIBRATION

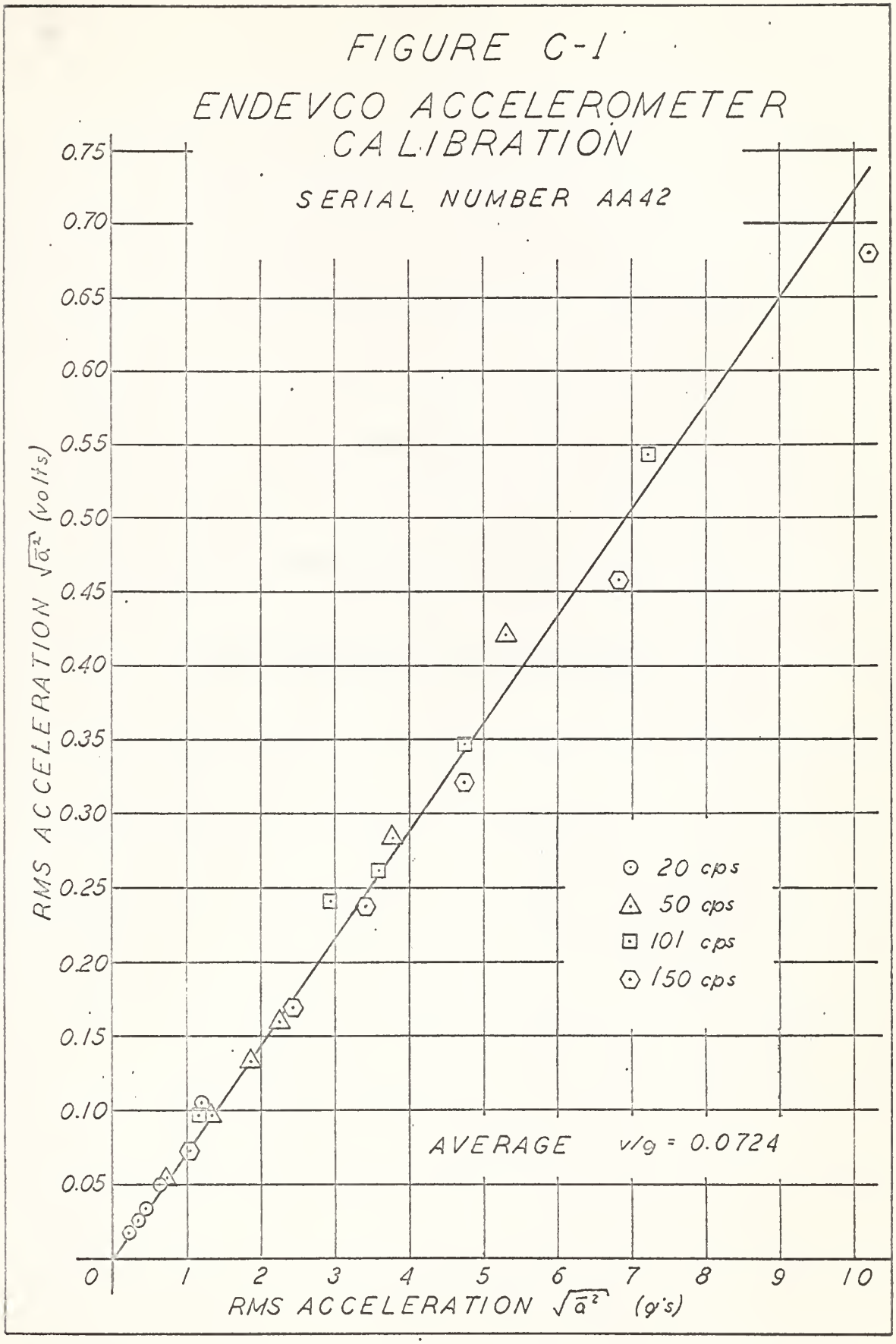

APPENDIX D

RESPONSE OF A CYLINDER

TO A

RANDOM AERODYNAMIC FORCING FUNCTION

APPENDIX D

RESPONSE OF A CYLINDER TO A RANDOM AERODYNAMIC FORCING FUNCTION

In the subcritical flow region about a circular cylinder, it has been experimentally established that the unsteady lift force is harmonic in nature. [1]. The exchange of energy between flow and cylinder is caused by the asymmetrical shedding of vortices in a periodic manner. Such an arrangement of vortices, which is in a pattern capable of maintaining itself in a perfect fluid, is known as a Karman vortex street. The cylinder response is harmonic, occurring at a constant Strouhal number of approximately 0.2, defined by the frequency of the shedding vortices.

The oscillating cylinder system may be represented by the following block diagram:

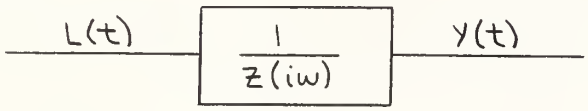

(1) with $y(t) = \frac{L(t)}{|Z(i\omega)|}$

$Z(i\omega)$ is the complex impedance of a second order system:

(2) $$Z(i\omega) = m[(i\omega)^2 + 2\beta\omega_N(i\omega) + \omega_N^2]$$
$$= m[\omega_N^2 - \omega^2 + i2\beta\omega\omega_N]$$

In the supercritical flow region ($R>10^5$), the flow in the wake of a cylinder becomes turbulent, and a defined vortex pattern is no longer present. The aerodynamic excitation is essentially non-periodic, and the structural oscillations behave like a response to a random excitation. The RMS amplitude of the response increases with increasing wind velocity. Equations (1) and (2) still define the system, but the random nature of

L(t) requires that a statistical analysis of the probelm, through use of Fourier integrals, be made.

The Fourier transform of L(t) is:

$$(3)\quad A(\omega) = \sqrt{\frac{2}{\pi}} \int_0^{\infty} L(t) e^{-i\omega t} dt;$$

and the inverse transform is:

$$(3a)\quad L(t) = \sqrt{\frac{2}{\pi}} \int_0^{\infty} A(\omega) e^{i\omega t} d\omega.$$

From equation (1), the system response becomes:

$$(4)\quad y(t) = \sqrt{\frac{2}{\pi}} \int_0^{\infty} \frac{A(\omega)}{|z(i\omega)|} e^{i\omega t} d\omega;$$

where:

$$(4a)\quad \frac{A(\omega)}{|z(i\omega)|} = \sqrt{\frac{2}{\pi}} \int_0^{\infty} y(t) e^{-i\omega t} d\omega.$$

For equations (3) and (4) to hold, the integrals $\int_{-\infty}^{+\infty} |L(t)|\, dt$ and $\int_{-\infty}^{+\infty} |y(t)|\, dt$ must converge, in addition to having L(t) and y(t) satisfy the Dirichlet condition of a finite number of maxima and minima. L(t) has been defined as a completely random function. Therefore, it is stationary in a statistical sense; that is, the ensemble averages of L(t) are independent of time. It is then permissible to truncate L(t) outside of the interval [-T,T], where this interval is adequate to give a good measure of system characteristics, in order to assure the validity of the Fourier transformation. Then:

$$\int_{-\infty}^{+\infty} |L(t)|\, dt = \int_{-T}^{+T} |L(t)|\, dt$$

which assures convergence. Similarly:

$$\int_{-\infty}^{+\infty} |y(t)|\, dt = \int_{-T}^{+T} |y(t)|\, dt.$$

Since this paper is concerned with the response of an oscillating cylinder rather than the forcing function, y(t) as indicated in equation (4) will be investigated in the manner followed in [1] and [3]. Consider the auto-correlation function [Ry(τ)]. Since:

$$\overline{y(t)} = \lim_{T \to \infty} \frac{1}{2T} \int_{-T}^{+T} y(t)\, dt,$$

and $\overline{y^2(t)} = \lim_{T\to\infty} \frac{1}{2T}\int_{-T}^{+T} y^2(t)\,dt;$

$R_y(\tau) = \overline{y(t)\,y(t+\tau)} = \lim_{T\to\infty} \frac{1}{2T}\int_{-T}^{+T} y(t)\,y(t+\tau)\,dt.$

Substituting equation (4) for $y(t+\tau)$ produces:

$$R_y(\tau) = \lim_{T\to\infty} \frac{1}{2T}\int_{-T}^{+T} y(t)\left[\frac{1}{\sqrt{2\pi}}\int_{-\infty}^{+\infty} \frac{A(\omega)}{|z(i\omega)|} e^{i\omega(t+\tau)}\,d\omega\right]dt;$$

which rearranged becomes:

$$R_y(\tau) = \lim_{T\to\infty} \frac{1}{2T}\int_{-\infty}^{+\infty} \frac{A(\omega)}{|z(i\omega)|} e^{i\omega\tau}\left[\frac{1}{\sqrt{2\pi}}\int_{-T}^{+T} y(t)\,e^{i\omega t}\,dt\right]d\omega.$$

Substituting equation (4a), with a sign change, for the bracketed quantity:

$$R_y(\tau) = \lim_{T\to\infty} \frac{1}{2T}\int_{-\infty}^{+\infty} \frac{A(\omega)}{|z(i\omega)|} e^{i\omega\tau}\left[\frac{A^*(\omega)}{|z(i\omega)|}\right]d\omega;$$

where $A^*(\omega)$ is the complex conjugate of $A(\omega)$. Since $y(t)$ is real, $A(\omega)A^*(\omega) = |A(\omega)|^2$, and:

$$R_y(\tau) = \lim_{T\to\infty} \frac{1}{2T}\int_{-\infty}^{+\infty} \frac{|A(\omega)|^2}{|z(i\omega)|^2} e^{i\omega\tau}\,d\omega$$

$$= \int_{-\infty}^{+\infty} \lim_{T\to\infty} \frac{1}{2T}\,\frac{|A(\omega)|^2}{|z(i\omega)|^2} e^{i\omega\tau}\,d\omega.$$

Let $\phi(\omega) = \lim_{T\to\infty} \frac{1}{T}|A(\omega)|^2$ be defined as the power spectral density of $\overline{L^2(t)}$. Then: $R_y(\tau) = \int_0^{\infty} \frac{\phi(\omega)}{|z(i\omega)|^2} e^{i\omega\tau}\,d\omega.$

This produces the mean square time average:

(5) $$R_y(0) = \overline{y^2(t)} = \int_0^{\infty} \frac{\phi(\omega)}{|z(i\omega)|^2}\,d\omega.$$

A similiar derivation from equation (3) gives:

(6) $$\overline{L^2(t)} = \int_0^{\infty} \phi(\omega)\,d\omega.$$

Plotting $\phi(\omega)$ against ω produces a curve, the area under which represents the mean square of the lift force as indicated in equation (6).

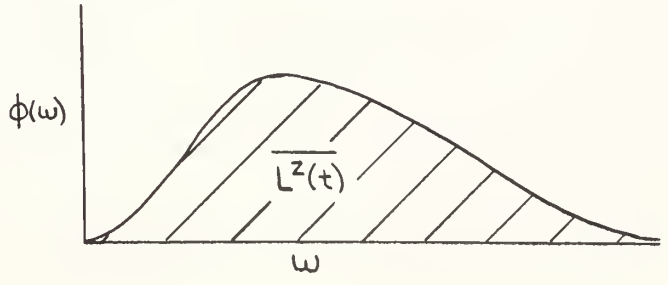

A similiar relationship exists between the plot of $\phi(\omega)/|z(i\omega)|^2$ versus ω, and the mean square of the system response $\overline{y^2(t)}$. However, the complex impedance affects $\overline{y^2(t)}$ in an interesting manner for a lightly damped system. From equation (2):

$$\frac{1}{|z(i\omega)|^2} = \frac{1}{m^2\left[(\omega_N^2-\omega^2)^2+4\beta^2\omega^2\omega_N^2\right]} = \frac{1}{m^2\omega_N^2\left[\left\{1-(\omega/\omega_N)^2\right\}^2+4\beta^2(\omega/\omega_N)^2\right]}.$$

Then equation (5) becomes:

$$\overline{y^2(t)} = \int_0^\infty \frac{\phi(\omega)}{m^2\omega_N^4\left[\left\{1-(\omega/\omega_N)^2\right\}^2+4\beta^2(\omega/\omega_N)^2\right]}\,d\omega.$$

If β is small, $\phi(\omega)$ can be assumed to vary at a much slower rate than the impedance term, with respect to frequency, near to the natural frequency of the cylinder. Then:

$$(7)\quad \overline{y^2(t)} = \frac{\phi(\omega_N)}{m^2\omega_N^2}\int_0^\infty \frac{1}{\left[\left\{1-(\omega/\omega_N)^2\right\}^2+4\beta^2(\omega/\omega_N)^2\right]}\,d\omega.$$

For ω near to ω_N, let $\omega = \omega_N+\varepsilon$ where ε is a small quantity. Then the following relationships hold:

$$d\omega = d\varepsilon$$
$$\omega/\omega_N = 1+\varepsilon/\omega_N$$
$$(\omega/\omega_N)^2 \doteq 1+2\varepsilon/\omega_N$$

Equation (7) now becomes:

$$\overline{y^2(t)} \doteq \frac{\phi(\omega_N)}{m^2\omega_N^4}\int_{-\omega_N}^\infty \frac{1}{\left[-2\varepsilon/\omega_N\right]^2+4\beta^2(1+2\varepsilon/\omega_N)}\,d\varepsilon$$

$$= \frac{\phi(\omega_N)}{m^2\omega_N^4}\int_{-\omega_N}^\infty \frac{1}{\varepsilon^2+\beta^2\omega_N^2}\,d\varepsilon,$$

neglecting higher order terms. Integrating:

$$(8)\quad \overline{y^2(t)} = \frac{\phi(\omega_N)}{m^2\omega_N^2}\,\frac{\pi}{4\omega_N}\,\frac{1}{\beta} = \text{Constant}\left(\frac{1}{\beta}\right).$$

For a lightly damped system, $\overline{y^2(t)}$ becomes large as ω approaches ω_N. Thus, the plot of equation (5) has the form:

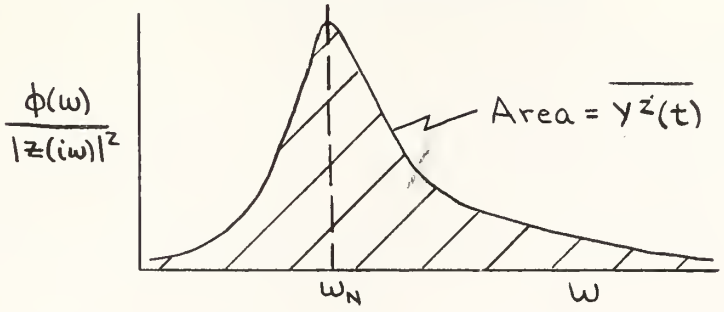

The principal response is to the narrow band of frequencies around ω_N, the contributions by more remote spectral components being of minor order. This tendency towards selective response may be likened to the action of a narrow band-pass filter that passes only those frequency components closely centered around a single value. The amplitude of the motion is determined by the summation of the spectral force components; however, the frequency response will be equal to the natural frequency of the cylinder.

In order to numerically predict the response of the smooth cylinder tested in this experiment. The results obtained in [5] may be employed. In that report, Dr. Fung defined the mean square lift force as:

(9) $$\overline{L^2(t)} = \int_0^\infty \phi(s)\,ds.$$

in the same manner as equation (6). In terms of ω, equation (9) becomes:

(10) $$\overline{L^2(t)} = \frac{d}{2\pi V}\int_0^\infty \phi(s)\,d\omega$$ for constant velocity.

Following the same derivation which led to equation (8), the response in terms of Strouhal number becomes:

$$\overline{y^2(t)} = \frac{1}{8m^2\omega_N^3}\,\frac{d}{V}\,\frac{1}{\beta}\,\phi(S_N) \qquad \text{where } S_N = \frac{\omega_N d}{2\pi V}.$$

In terms of the normalized power spectral density [$\phi_n(S_N)$], this is:

$$(11)\quad \overline{y^2(t)} = q_b^2 A^2 \overline{C_L^2}\left[\frac{1}{8m^2\omega_N^3}\frac{d}{V}\frac{1}{\beta}\phi_n(S_N)\right].$$

A typical RMS value of C_L for a circular cylinder in supercritical flow is 0.14. [5]. Substituting the model dimension values of Appendix F and a β of 0.0183, equation (11) becomes for this experiment:

$$(12)\quad \overline{y^2(t)} = 0.376\, q_b^2 \frac{1}{V}\frac{1}{f_N^3}\phi_n(S_N)$$

with y in inches,
q_b psf,
V fps,
f_N cps.

The reference curve which was fitted to the measured spectra in [5] is used to define $\phi_n(S_N)$.

$$\phi_n(\eta) = \frac{\ell}{d}\,\frac{2(1+3\eta^2)}{(1+\eta^2)^2}$$

where ℓ = scale of turbulence,
d = diameter,
ℓ/d = 2.4 [5],
$\eta = 2\pi\frac{\ell}{d}S = 15.08S$.

This function is plotted in Figure D-1. Table D-1 lists the results of equation (12) for the model natural frequencies tested. The RMS accelerations obtained from these results are plotted in Figure D-2 as a function of tunnel dynamic pressure. For purposes of comparison, the test results for the smooth cylinder configuration B are included in Figure D-2.

FIGURE D-1

NORMALIZED POWER SPECTRAL DENSITY

$$\phi_n(\eta) = \frac{\ell}{d} \frac{2(1 + 3\eta^2)}{(1. + \eta^2)^2}$$

$$\eta = 2\pi \frac{\ell}{d} S$$

$$\frac{\ell}{d} = 2.4$$

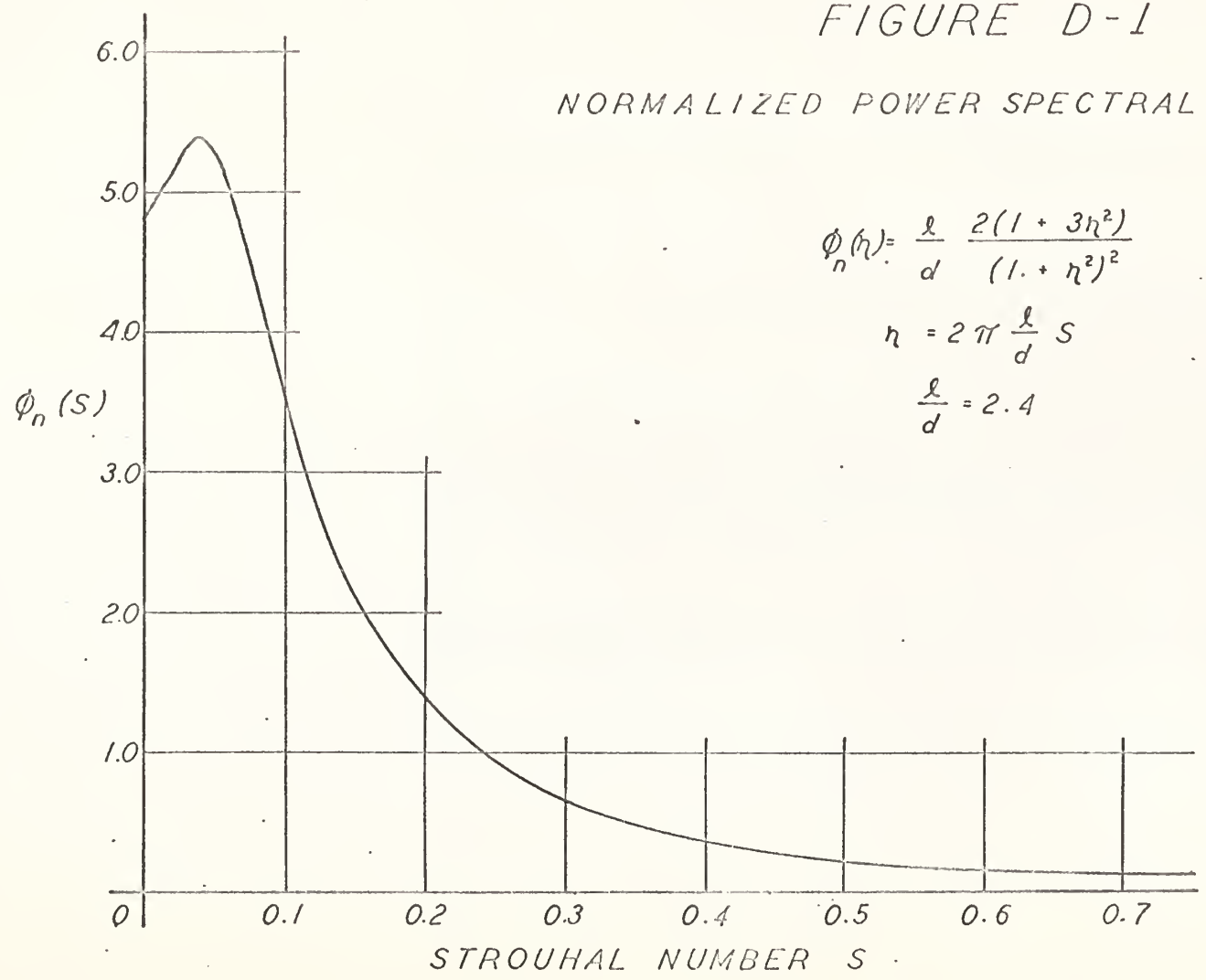

TABLE D-I

Smooth Cylinder Response Prediction

f_N (cps)	q (psf)	$\sqrt{\overline{y^2}}$ (in)	$\sqrt{\overline{a^2}}$ (g's)
20	10	.0139	.570
	20	.0266	1.092
	30	.0372	1.52
	40	.0472	1.93
	50	.0555	2.27
	60	.0642	2.62
	100	.0925	3.78
30	10	.00598	.550
	20	.0125	1.15
	30	.0185	1.70
	40	.0240	2.22
	50	.0292	2.69
	60	.0340	3.13
	100	.0506	4.66
40	10	.00312	.512
	20	.00691	1.13
	30	.0106	1.74
	40	.01405	2.30
	50	.01735	2.85
	60	.0206	3.38
	100	.0321	5.25
50	10	.00183	.468
	20	.00411	1.05
	30	.00648	1.66
	40	.00996	2.29
	50	.0112	2.87
	60	.0136	3.48
	100	.0219	5.59

FIGURE D-2

SMOOTH CYLINDER RESPONSE COMPARISON

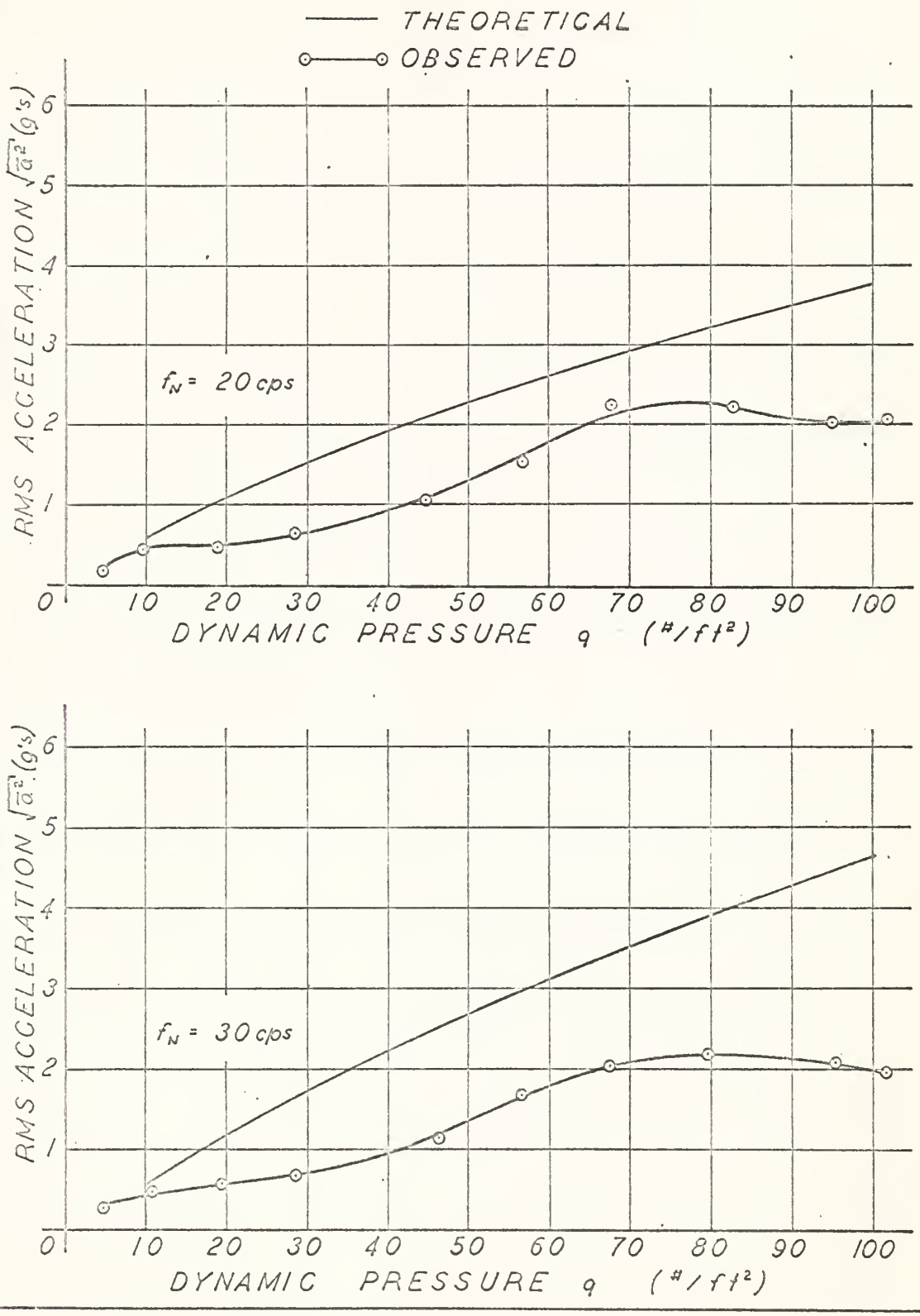

FIGURE D-2

SMOOTH CYLINDER RESPONSE COMPARISON

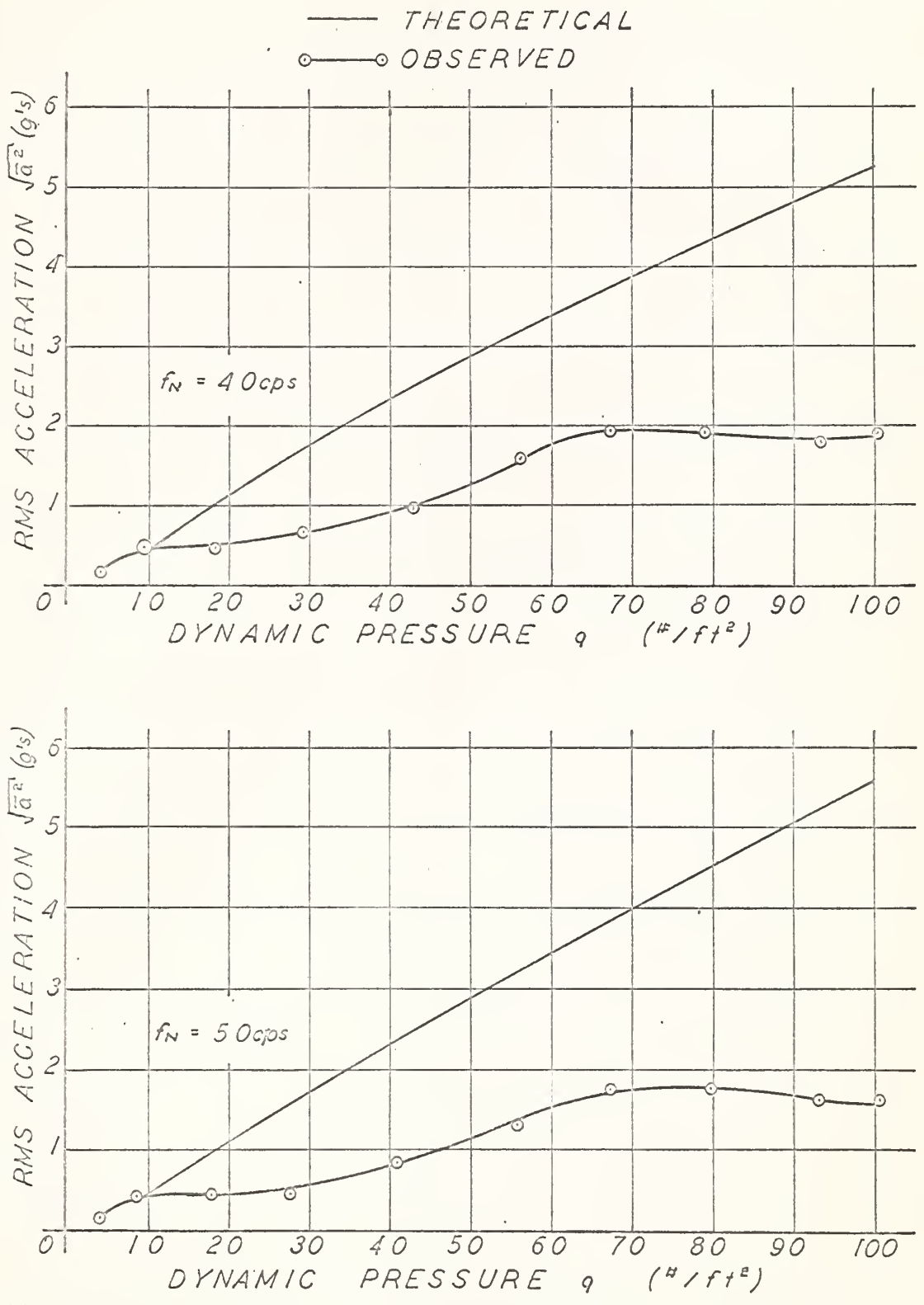

APPENDIX E

TEST DATA AND RESULTS

APPENDIX E

TEST DATA AND RESULTS

CONFIGURATION A

Smooth Cylinder Base Pressure Test

TOTAL HEAD (cm H_2O)	$-\Delta P_B$ (cm Si)	T (^oF)	V (fps)	$\nu \times 10^{-4}$ (ft^2/sec^2)	q (psf)	$-C_{P_B}$	R $\times 10^{-5}$
4.94	3.15	92	89	1.747	9.52	0.5524	2.149
10.16	5.42	94	129	1.767	19.59	0.4483	3.080
14.94	8.10	98	156	1.794	28.80	0.4571	3.668
20.46	11.50	101	182	1.821	39.44	0.4767	4.217
24.62	13.90	102	200	1.834	47.46	0.4794	4.600
29.92	16.97	103	218	1.842	57.68	0.4819	4.993
34.63	19.68	106	235	1.856	66.75	0.4831	5.342
39.43	22.79	109	253	1.870	76.02	0.4926	5.708
44.58	25.65	112	270	1.890	85.94	0.4900	6.027
49.43	29.20	116	284	1.912	95.29	0.5053	6.266
51.70	30.44	119	290	1.926	99.67	0.5033	6.352
52.62	31.46	121	293	1.933	101.44	0.5124	6.395

CONFIGURATION D

Proposed Fix

ℓ_B = 9.75 in., f_N = 20 cps, f_{AVE} = 21.7 cps.

TOTAL HEAD (cm H_2O)	T (^oF)	RMS g (volts)	V (ft/sec)	q (psf)	$\sqrt{a^2}$ (g's)
0.50	64	0.0185	28.5	0.962	0.256
2.00	66	0.022	57	3.85	0.304
4.00	67	0.023	81	7.70	0.318
5.00	68	0.021	90	9.62	0.290
9.74	69	0.031	126	18.85	0.428
14.07	70	0.040	151	27.05	0.554
19.30	72	0.064	177	37.20	0.884
23.41	72	0.079	196	45.10	1.09
28.74	74	0.095	218	55.35	1.31
33.37	76	0.110	233	64.2	1.52
38.77	78	0.125	251	74.6	1.73
42.90	80	0.110	264	82.6	1.52
47.50	84	0.110	278	91.5	1.52
51.49	86	0.120	289	99.0	1.66
53.06	99	0.120	294	102.2	1.66

CONFIGURATION B

Smooth Cylinder Oscillating

TOTAL HEAD (cm H_2O)	T (^oF)	RMS g (volts)	V (fps)	q (psf)	$\sqrt{\overline{a^2}}$ (g's)	R x 10^{-5}	
2.59	76	0.013	66	4.98	0.180	2.50	
5.00	68	0.029	90	9.65	0.401	2.29	
9.81	72	0.035	127	18.9	0.484	3.20	
14.76	77	0.045	155	28.4	0.623	3.84	
23.14	80	0.078	193	44.5	1.08	4.72	
29.55	82	0.11	218	56.9	1.52	5.30	
34.95	84	0.16	237	67.3	2.21	5.74	
42.84	87	0.16	264	82.6	2.21	6.32	
49.22	94	0.145	284	95.0	2.01	6.65	
52.93	98	0.15	293	101.8	2.08	6.77	f_N = 20 cps f_{AVG} = 25.6 cps
2.59	75	0.019	66	4.98	0.262	2.50	
5.29	82	0.032	94	10.19	0.443	2.29	
9.98	88	0.040	128	19.2	0.554	3.06	
14.96	91	0.045	156	28.8	0.662	3.68	
23.95	92	0.08	197	46.1	1.105	4.63	
29.49	93	0.12	218	56.8	1.66	5.11	
35.14	95	0.145	238	67.6	2.00	5.56	
41.40	98	0.155	259	79.7	2.14	5.98	
49.61	101	0.15	285	95.6	2.08	6.50	
52.91	104	0.14	293	101.8	1.935	6.64	f_N = 30 cps f_{AVG} = 33.9 cps
2.59	74	0.008	66	4.98	0.1105	2.50	
5.07	91	0.032	91	9.77	0.443	2.15	
9.65	94	0.033	126	18.59	0.456	2.95	
15.52	96	0.044	159	29.85	0.608	3.45	
22.72	98	0.070	191	43.7	0.969	4.12	
29.30	98	0.115	217	56.4	1.59	4.98	
35.12	100	0.140	238	67.6	1.935	5.39	
41.31	104	0.140	259	79.5	1.935	5.86	
48.69	108	0.130	282	93.8	1.80	6.32	
52.44	110	0.140	292	100.9	1.935	6.49	f_N = 40 cps f_{AVG} = 41.7 cps
2.59	73	0.0095	66	4.98	0.131	2.50	
4.87	97	0.03	89	9.39	0.415	2.06	
9.68	98	0.032	126	18.62	0.443	2.91	
14.61	100	0.034	155	28.2	0.470	3.56	
21.48	102	0.062	187	41.4	0.859	4.26	
29.53	103	0.098	218	56.9	1.35	4.95	
35.24	105	0.130	239	68.0	1.79	5.40	
41.79	108	0.130	261	80.5	1.79	5.84	
48.41	111	0.120	281	93.4	1.66	6.23	
52.64	114	0.120	292	101.2	1.66	6.44	f_N = 50 cps f_{AVG} = 60 cps

CONFIGURATION C

Cylinder with Flanges

TOTAL HEAD (cm H_2O)	T (^oF)	RMS g (volts)	f (cps)	V (fps)	q (psf)	$\sqrt{a^2}$ (g's)	S	
2.0	66	0.095	25	56	3.85	1.31	0.186	
4.0	68	0.075	23.5	80	7.70	1.04	0.122	
5.20	66	0.08	37	93	10.0	1.11	0.165	
10.00	71	0.17	51.5	129	19.28	2.35	0.166	
15.04	74	0.32	61	157	29.0	4.42	0.161	
18.30	76	0.25	73	173	35.3	3.45	0.176	
24.09	78	0.3	78	198	46.5	4.14	0.164	
29.18	84	0.42	92.5	217	56.2	5.80	0.177	
32.98	88	0.55	100	230	63.5	7.60	0.181	
36.18	92	0.75	109	244	71.0	10.36	0.186	f_N = 20 cps
2.00	65	0.036	30	56	3.85	0.499	0.224	
4.00	67	0.24	33	80	7.70	0.332	0.172	
5.20	68	0.18	30	92	10.0	2.49	0.136	
10.08	70	0.19	50	129	19.4	2.63	0.1615	
14.89	72	0.32	61.5	156	28.65	4.43	0.1645	
18.30	73	0.32	66.5	173	35.3	4.43	0.1605	
23.39	75	0.35	76.5	195	45.0	4.84	0.163	
29.05	80	0.42	91	216	56.0	5.81	0.176	
32.48	82	0.6	100	229	62.6	8.30	0.182	
34.88	88	0.71	104	237	67.2	9.82	0.183	
36.62	91	0.9	107	243	70.6	12.45	0.1835	f_N = 30 cps
2.00	80	0.025	76.5	56	3.85	0.346	0.567	
4.00	81	0.08	36	80	7.70	1.105	0.187	
5.20	81	0.3	40.5	92	10.0	4.15	0.183	
10.79	83	0.32	56	133	20.75	4.43	0.175	
15.46	85	0.38	67	159	29.8	5.25	0.175	
19.80	87	0.36	76.5	180	38.2	4.99	0.176	
24.46	89	0.41	81.5	199	47.2	5.67	0.170	
29.36	93	0.53	101	217	56.6	7.33	0.194	
33.68	96	0.72	104	233	64.9	9.95	0.186	
36.26	98	0.86	106	242	70.0	11.9	0.183	f_N = 40 cps
2.00	82	0.032	79.5	56	3.85	0.443	0.591	
4.00	84	0.04	70.5	80	7.70	0.554	0.367	
5.20	86	0.071	40.5	92	10.0	0.980	0.183	
10.26	86	0.32	50	129	19.75	4.43	0.161	
14.91	88	0.35	65	156	28.75	4.84	0.174	
19.81	90	0.42	75	180	38.2	5.81	0.173	
24.99	92	0.48	82	201	48.1	6.64	0.170	
30.67	94	0.55	92	222	59.2	7.60	0.172	
33.86	97	0.7	104	234	65.4	9.69	0.185	
37.30	98	0.84	103	246	71.8	11.6	0.174	f_N = 50 cps

Typical Brush Recorder tracings of the static tests to determine system natural frequency (f_N) and damping (β).

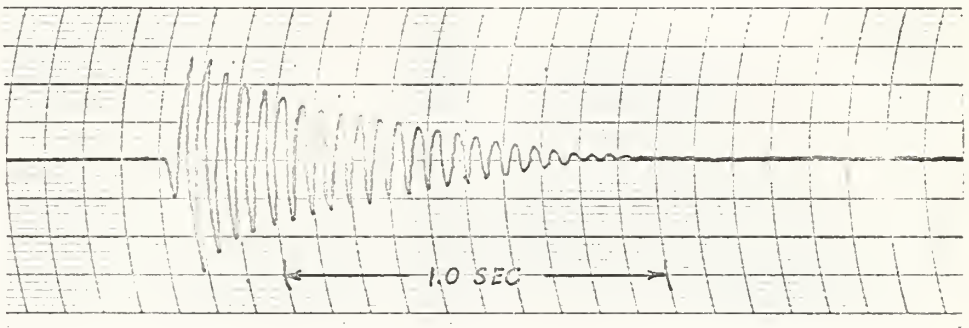

$\ell_B = 10''$ $f_N = 19.75$ cps $\beta = 0.0192$

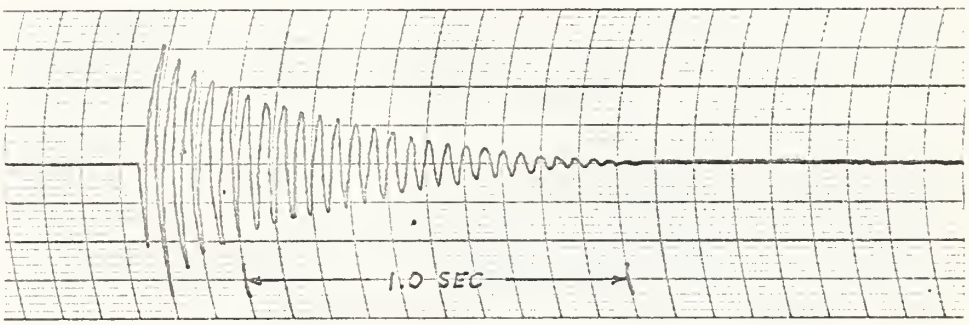

$\ell_B = 9.5''$ $f_N = 20.75$ cps $\beta = 0.0175$

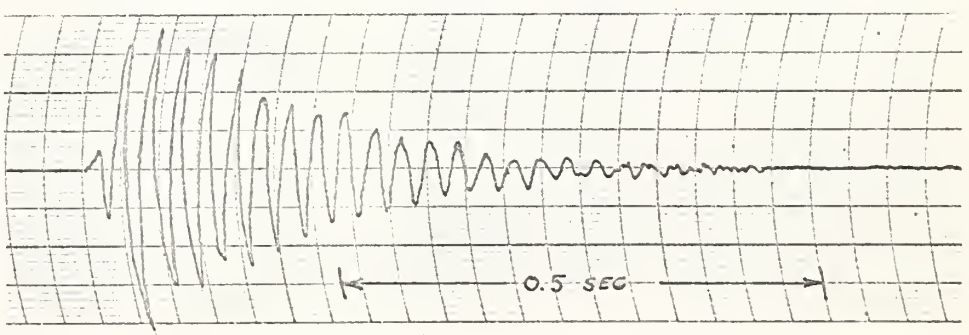

$\ell_B = 6.0''$ $f = 34.5$ cps β - poorly defined

Typical Brush Recorder tracings of the response of the smooth cylinder (configuration B), showing the random frequency and amplitude.

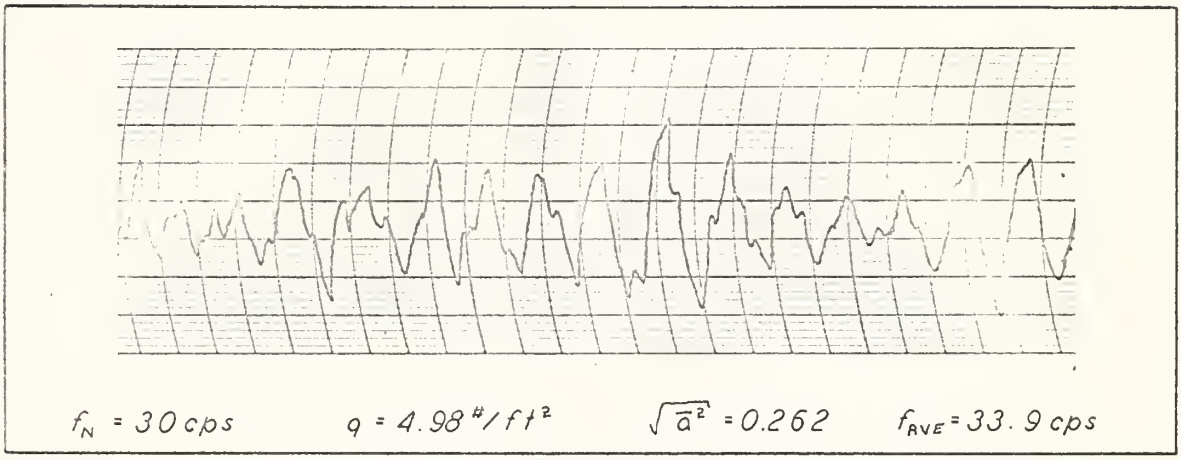

$f_N = 30$ cps $q = 4.98\ ^{\#}/ft^2$ $\sqrt{\overline{a^2}} = 0.262$ $f_{AVE} = 33.9$ cps

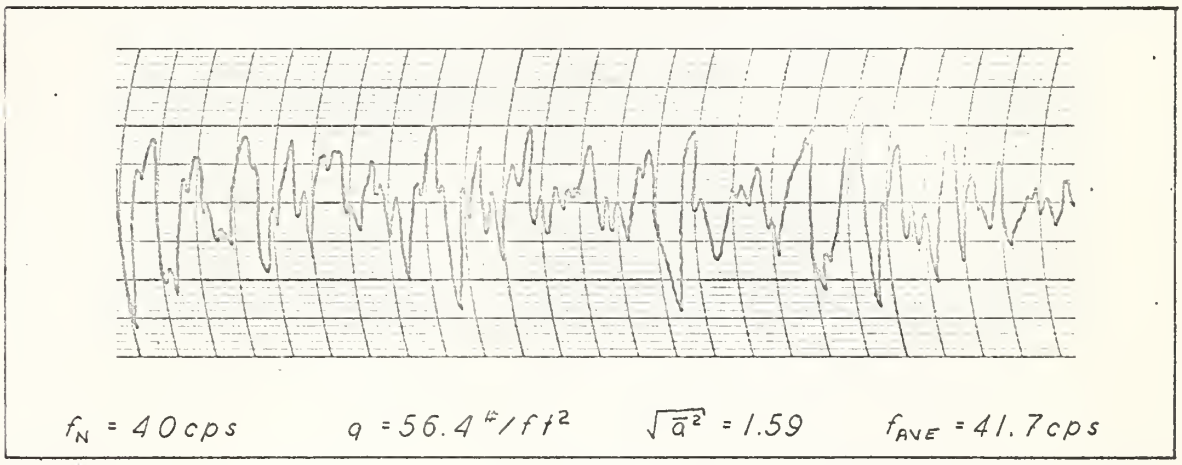

$f_N = 40$ cps $q = 56.4\ ^{\#}/ft^2$ $\sqrt{\overline{a^2}} = 1.59$ $f_{AVE} = 41.7$ cps

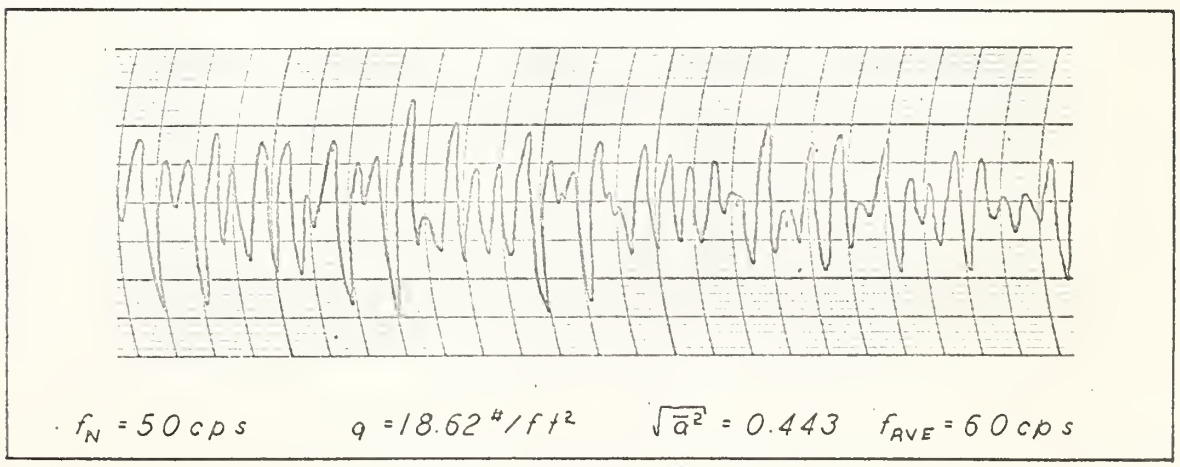

$f_N = 50$ cps $q = 18.62\ ^{\#}/ft^2$ $\sqrt{\overline{a^2}} = 0.443$ $f_{AVE} = 60$ cps

Typical Brush Recorder tracings of the response of the cylinder with flanges (configuration C), showing the random amplitude and harmonic frequency.

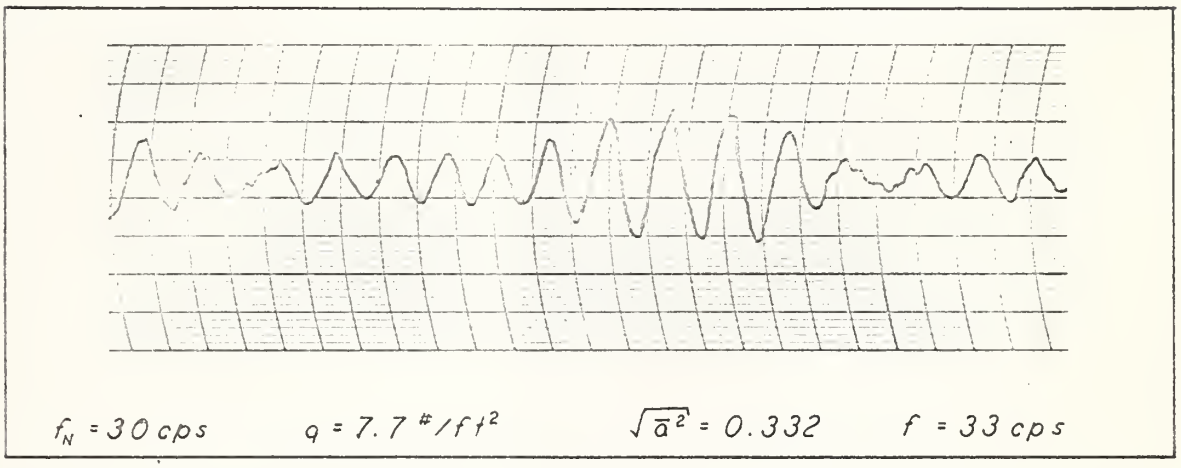

f_N = 30 cps q = 7.7 #/ft² $\sqrt{\overline{a^2}}$ = 0.332 f = 33 cps

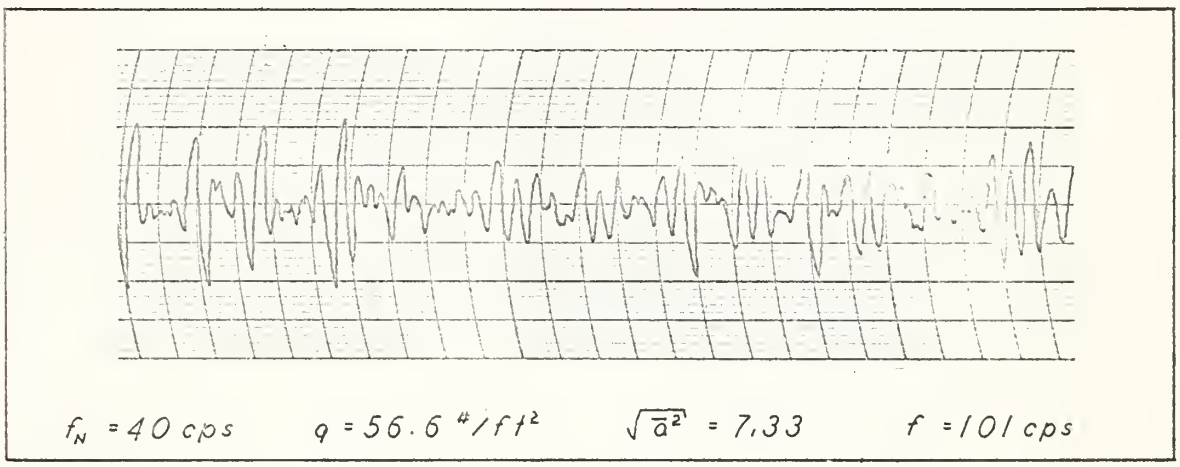

f_N = 40 cps q = 56.6 #/ft² $\sqrt{\overline{a^2}}$ = 7.33 f = 101 cps

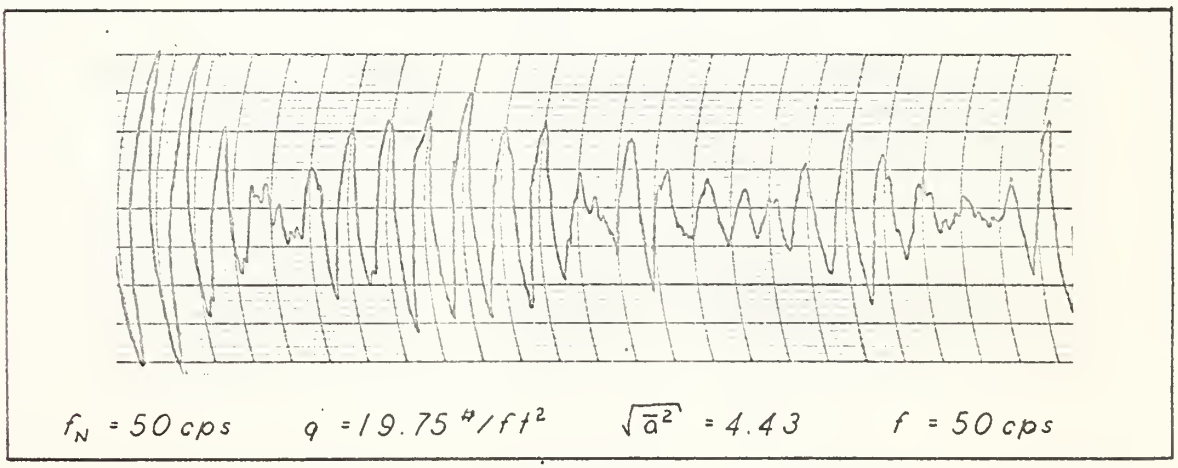

f_N = 50 cps q = 19.75 #/ft² $\sqrt{\overline{a^2}}$ = 4.43 f = 50 cps

Typical Brush Recorder tracings of the response of the model with flanges at both stagnation points (configuration D), showing response similar to that of a smooth cylinder. f_N = 20 cps f_{AVE} = 21.7 cps

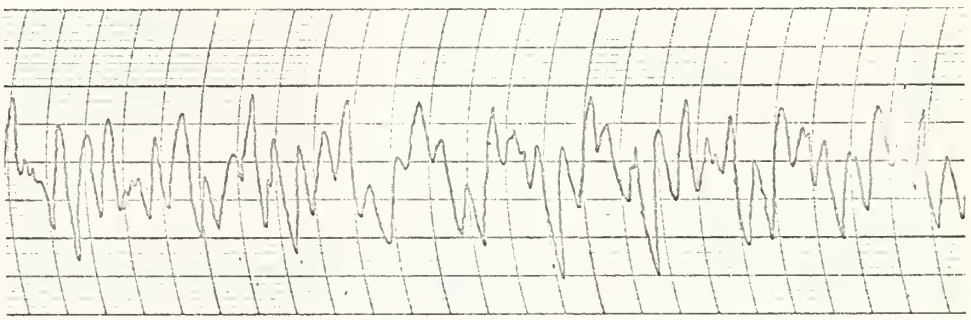

$q = 9.62\ ^{\#}/ft^2$ $\sqrt{\overline{a^2}} = 0.29$

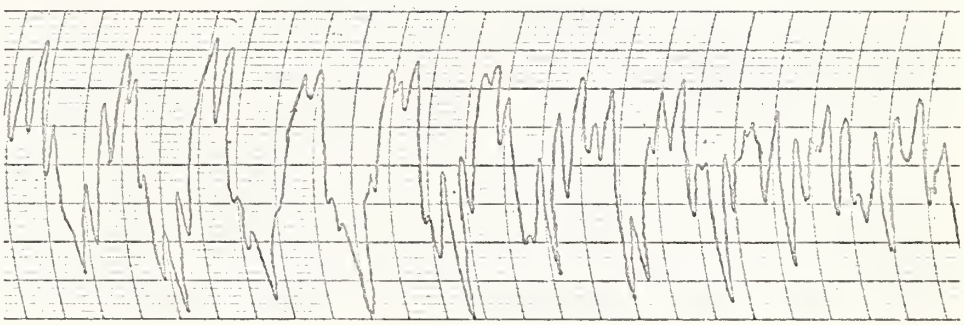

$q = 45.1\ ^{\#}/ft^2$ $\sqrt{\overline{a^2}} = 1.09$

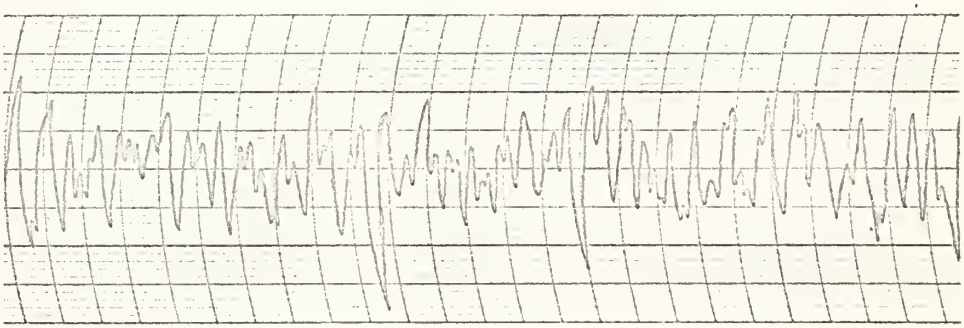

$q = 99.0\ ^{\#}/ft^2$ $\sqrt{\overline{a^2}} = 1.66$

APPENDIX F

MODEL SPECIFICATIONS

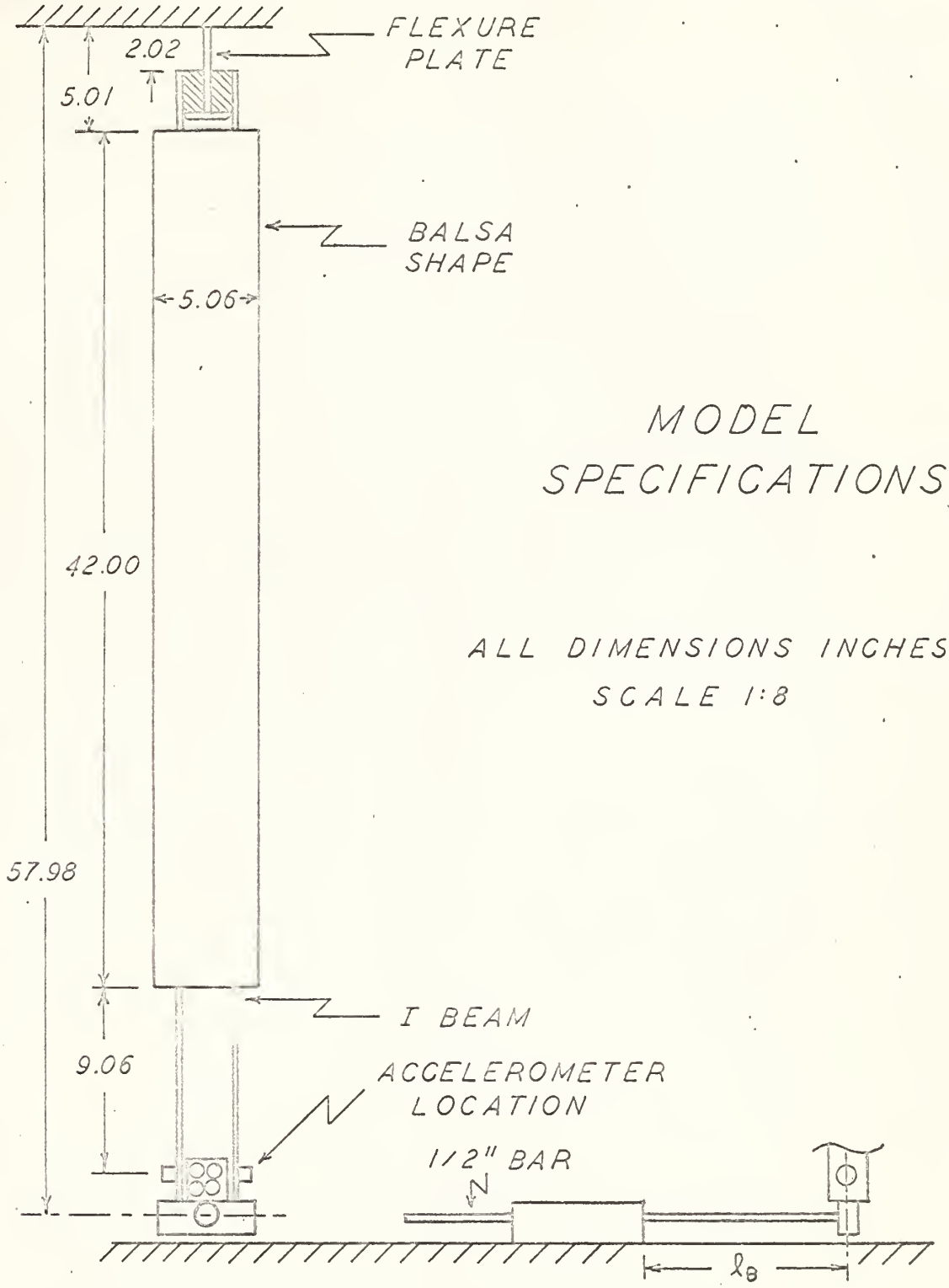

MODEL SPECIFICATIONS

ALL DIMENSIONS INCHES

SCALE 1:8

WEIGHTS:

METAL	9.55#
WOOD	4.29#
TOTAL	13.84#

$(EI)_B = 9.21 \times 10^5$ # in^2

$(EI)_F = 5283$ # in^2